Macrocyclic Allylic Sulfone as A Universal Comonomer in Organocatalyzed Photocontrolled Radical Copolymerization with Vinyl Monomers

Wenqi Wang, Brayan Rondon, Zeyu Wang, Junpeng Wang, and Jia Niu*

ABSTRACT

Radical copolymerization of vinyl monomers and cyclic monomers is a versatile approach to degradable vinyl plastics. Despite recent advances, a class of "universal" cyclic monomers that possess broad reactivities with various types of vinyl monomers remains elusive. Herein, we report a general method for the organocatalyzed photocontrolled radical ring-opening cascade copolymerization (rROCCP) of macrocyclic allylic sulfone and various types of vinyl monomers, including acrylates, acrylamides, styrene, and methacrylate. Catalyzed by Eosin Y under visible light irradiation, the copolymerization of macrocyclic allylic sulfone and acrylic monomers displayed near unity comonomer reactivity ratios by fitting the copolymer composition to the Beckingham-Sanoya-Lynd integrated model. Macrocyclic allylic sulfone was also successfully copolymerized with styrene (r_1=3.02 and r_{St}=0.35) or methyl methacrylate (r_1=0.18 and r_{MMA}=5.81) to generate degradable polystyrene and poly(methyl methacrylate). These degradable vinyl copolymers exhibited tunable thermal properties correlated with the incorporation of the degradable main-chain diester motif. The unprecedented reactivities that macrocyclic allylic sulfone demonstrated in the organocatalyzed photocontrolled rROCCP provide a general approach to a wide range of degradable vinyl plastics with various structures and functions.

INTRODUCTION

The global annual production of plastics has increased dramatically over the past four decades and is now approaching 400 million metric tons, approximately 70 percent of which are vinyl plastics.[1] Thanks to their low cost, high durability, and easy processability, vinyl plastics have been widely used in various types of applications, including packaging, construction materials, adhesives, coatings, and synthetic fibers. However, the half-lives of many types of commodity vinyl plastics are much longer than necessary for their applications, leading to the accumulation of plastic waste in the environment.[2-6] A potential solution to this challenge is to achieve polymer degradation at the end of their life cycle by incorporating labile functionalities into the main chain of vinyl polymers.

Since the first report in the 1960s,[7] radical ring-opening polymerization has emerged as a powerful approach to incorporating labile functionalities, such as ester, disulfide, or carbonate, into the backbone of vinyl polymers.[8-11] Pioneered by Bailey[12] and Endo,[13] cyclic ketene acetals[14-17] have been extensively investigated to copolymerize with various vinyl monomers but were often found to have non-optimal copolymerization reactivities and poor rate of incorporation. Recently reported by Roth[18] and Gutekunst[19] in 2019, dibenzo[*c,e*]oxepane-5-thiones (DOTs)[20-24] have shown successful copolymerization with acrylates, acrylamides, acrylonitrile, maleimide, and styrene to synthesize degradable linear copolymers and degradable polymer networks. However, copolymerization of DOTs and methacrylates remains challenging.

Polymerization regulated by light serves as a great alternative to thermally-initiated polymerization due to its economic and ubiquitous nature.[25-27] Integrated with reversible deactivation radical polymerization,[28-30] photocontrolled radical polymerization could produce macromolecular structures with defined molecular weight and architecture under mild conditions. Light-mediated polymerization at low temperatures (-20 to 50 ºC) also enabled the fine-tuning of

polymer tacticity as well as composition.[31-32] In 2021, we reported that the *fac*-Ir(ppy)$_3$-mediated photocontrolled radical ring-opening cascade copolymerization (rROCCP) of macrocyclic allylic sulfone and acrylic monomers produced degradable vinyl copolymers with favorable reactivities.[33] However, the potential toxicity and challenge in the removal of transition-metal photocatalysts may preclude the use of these degradable vinyl copolymers in biomedical and electronic applications. Therefore, we explored organocatalyzed photocontrolled rROCCP.[34-38] We demonstrated that macrocyclic allylic sulfone serves as a "universal" cyclic monomer in organocatalyzed photocontrolled rROCCP and can copolymerize with a variety of vinyl monomers, including acrylates, acrylamides, styrene, and methacrylate, incorporating degradability to otherwise nondegradable vinyl polymers (Scheme 1).

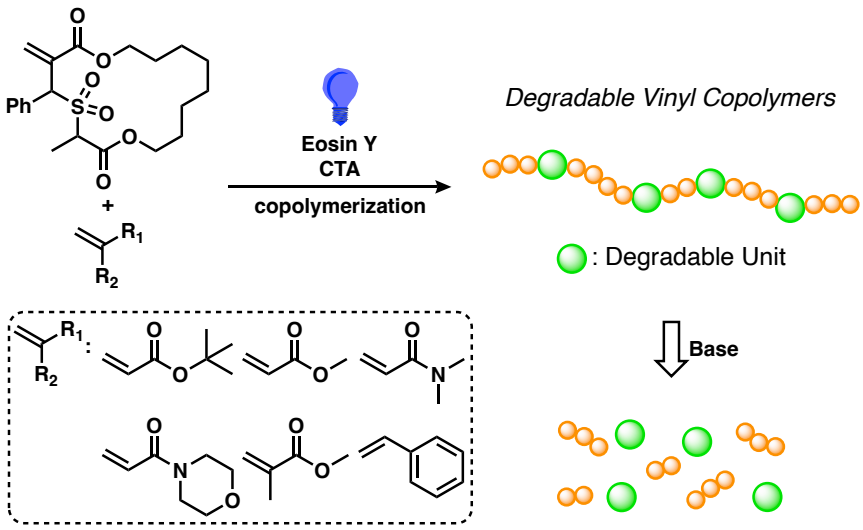

Scheme 1. Organocatalyzed photocontrolled rROCCP of macrocyclic allylic sulfone and a variety of vinyl monomers generates degradable vinyl copolymers.

RESULTS AND DISCUSSION

Organocatalyzed photocontrolled homopolymerization of macrocyclic allylic sulfone. Adopting the organocatalyzed photoinduced electron/energy transfer-radical addition/fragmentation chain transfer (PET-RAFT) method reported by Xu and Boyer,[36] the homopolymerization of macrocyclic allylic sulfone **1** was first investigated (Figure 1A). The polymerization of **1** ($[M]_0$ = 0.2 M) was initially attempted with the control of Eosin Y (EY, $[EY]_0/[M]_0$ = 200 ppm) and chain transfer agent **CTA1** ($[M]_0/[I]_0$ = 50/1) under λ_{max} = 450 nm blue light irradiation (Figure 1A). The reaction reached 20% conversion in 10 hours and yielded well-defined polymer **P-1** with a number average molecular weight ($M_n^{(SEC)}$) of 3.0 kg mol^{-1} and dispersity ($Đ$) of 1.08 by size-exclusion chromatography (SEC) (Table S1, entry 1). Further optimization of initial monomer concentration ($[M]_0$) and photocatalyst loading ($[EY]_0/[M]_0$) revealed that the polymerization reached 68% conversion with $[M]_0$ = 0.5 M and $[EY]_0/[M]_0$ = 1000 ppm, affording **P-1** with $M_n^{(SEC)}$ of 7.7 kg mol^{-1} and $Đ$ of 1.13 in 4 hours (Table S1, entry 5). Next, we examined the living/controlled characteristics of the organocatalyzed radical homopolymerization of **1**. The kinetic study of the polymerization of **1** exhibited first-order kinetics (Figure 1B). The observed rate constant for **1** was calculated as k_1 = 0.11 h^{-1}. At the feeding monomer/initiator ($[M]_0/[I]_0$) ratio of 50/1, linear growth of $M_n^{(SEC)}$ of **P-1** with respect to monomer conversion was observed, and low dispersity ($Đ$ < 1.2) was maintained throughout the polymerization (Figure 1C), indicating an excellent control of the polymerization. The proton nuclear magnetic resonance (^{1}H NMR) analysis of well-defined polymer **P-1-8k** showed an equal stoichiometry of the α-chain end (1.21 ppm) and the ω-chain end (3.36 ppm), suggesting a high chain-end fidelity (Figure S1). The molecular weight of **P-1-8k** determined by the ^{1}H NMR integration ratio of the polymer backbone to the ω-chain end was 8.9 kg mol^{-1}, which was consistent with the theoretical value based on the $[M]_0/[I]_0$ ratio and monomer conversion ($M_n^{(theo)}$

= 8.9 kg mol^{-1}) as well as the value obtained from SEC analysis ($M_n^{(SEC)}$ = 8.3 kg mol^{-1}) (Figure S1). Matrix-assisted laser desorption/ionization time-of-flight (MALDI-TOF) mass spectrometry analysis of a lower molecular weight polymer **P-1-3k** showed discrete peaks spaced by 334.2 g mol^{-1}, which corresponds to the mass of the repeating unit (Figure 1D). These peaks were unambiguously assigned to the discrete oligomers with a propionic acid group as the α-chain end and an ethyl trithiocarbonate group as the ω-chain end, respectively, consistent with the ^{1}H NMR results. Encouraged by the excellent end-group fidelity, a block-copolymerization experiment was further conducted. First, organocatalyzed radical homopolymerization of **1** yielded the macroinitiator **P-1-8k** ($M_n^{(SEC)}$ = 7.9 kg mol^{-1}, $Đ$ = 1.13), which was then used to polymerize methyl acrylate (MA) to generate the block copolymer **P-1-*b*-PMA** ($M_n^{(SEC)}$ = 12.8 kg mol^{-1}, $Đ$ = 1.13, Figure 1E). A clear shift of the original unimodal peak to the higher molecular weight region was observed on the SEC after block copolymerization, suggesting the formation of a diblock copolymer. Taken together, these results supported that the organocatalyzed photocontrolled homopolymerization of **1** maintained excellent control throughout the polymerization.

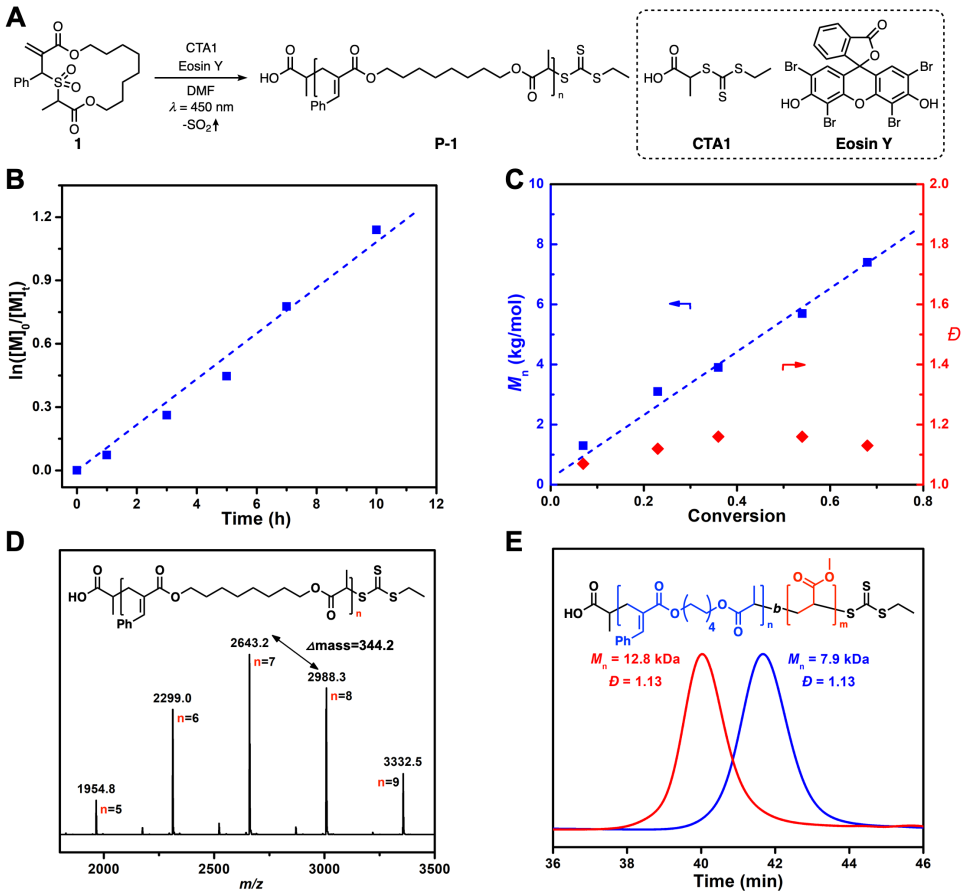

Figure 1. (A) Organocatalyzed photocontrolled homopolymerization of **1**. (B) Kinetic plot of $\ln([M]_0/[M]_t)$ versus reaction time, where $[M]_0$ is the initial monomer concentration and $[M]_t$ is the monomer concentration at a given time t. (C) Plots of M_n and $Đ$ of **P-1** as a function of monomer conversion. (D) MALDI-TOF analysis of **P-1-3k**. Each peak corresponds to a discrete oligomer that consists of the α- and ω-chain ends, the number of repeating units multiplied by its molar mass, and a sodium cation. A set of minor peaks was observed, which corresponded to the loss of the ω-chain end of **P-1-3k** during the MALDI-TOF measurement. (E) SEC analysis of the formation of diblock copolymer **P-1-*b*-PMA** from the extension of a macroinitiator **P-1-8k** by MA.

Scheme 2. Degradable Vinyl Copolymers via Organocatalyzed Photocontrolled rROCCP and Their Degradation under Basic Condition.

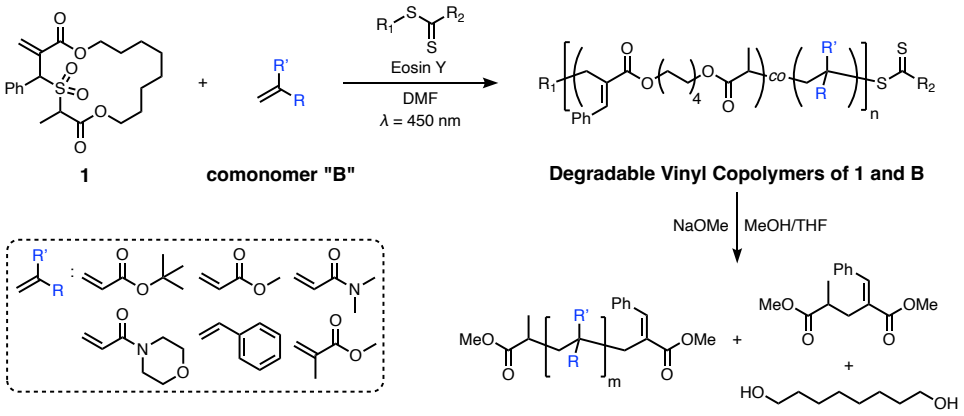

Table 1. Organocatalyzed Photocontrolled rROCCP of **1** and Vinyl Monomers.

Entry[a]	**B**	[**B**]:[**1**]:[CTA]	*conv.*[b]	f_1^0	$F_1^{(end)b}$	$M_n^{(SEC)}$ (kg mol^{-1})[c]	$Đ^c$
1	*t*BA	100:10:1	90%	0.09	0.09	11.3	1.11
2	*t*BA	200:10:1	90%	0.05	0.05	22.5	1.15
3	*t*BA	200:20:1	92%	0.09	0.09	23.9	1.25
4	*t*BA	200:66:1	90%	0.25	0.25	24.4	1.26
5	DMA	100:10:1	92%	0.09	0.09	8.0	1.18
6	DMA	200:10:1	94%	0.05	0.05	15.7	1.29
7	DMA	200:20:1	95%	0.09	0.09	14.7	1.28
8	DMA	200:66:1	73%	0.25	0.25	13.6	1.31
9	MA	100:10:1	78%	0.09	0.09	7.8	1.10
10	MA	200:20:1	91%	0.09	0.09	17.9	1.24
11[d]	NAM	100:10:1	83%	0.09	0.09	7.7	1.12
12[d]	NAM	200:20:1	87%	0.09	0.09	19.2	1.22
13[e]	St	100:10:1	44%	0.09	0.16	8.8	1.23
14[e]	St	200:10:1	51%	0.05	0.07	13.0	1.35

15[e]	St	200:20:1	41%	0.09	0.15	14.0	1.31
16[e]	MMA	100:10:1	77%	0.09	0.01	11.5	1.36
17[e]	MMA	50:50:1	62%	0.50	0.25	7.4	1.26

[a]The reactions were performed at 25 °C under nitrogen with an 18 W blue LED light (λ_{max} = 450 nm) for 5 hours. $[M]_0$ = 0.5 M; $[EY]_0/[M]_0$ = 1000 ppm. [b]Monomer conversion and $F_1^{(end)}$ were determined by ^{1}H NMR spectroscopy. [c]M_n and $Đ$ were determined by SEC analysis calibrated to polystyrene standards. [d]Reaction time: 75 minutes. [e]Reaction time: 50 hours.

Table 2. Reactivity Ratios of **1** and Vinyl Monomers and Degradation of Vinyl Copolymers.

Entry[a]	**B**	r_1	r_B	f_1^0	$F_1^{(end)b}$	$M_n^{(SEC)}$ (kg mol^{-1})[c]	$Đ^c$	Degraded $M_n^{(SEC)}$ (kg mol^{-1})[c]	Degraded $Đ^c$
1	*t*BA	1.04	0.96	0.09	0.09	11.3	1.11	1.8	1.46
2	MA	1.02	0.98	0.09	0.09	7.8	1.10	1.3	1.55
3	DMA	0.98	0.93	0.09	0.09	8.0	1.18	1.0	1.13
4	NAM	0.99	1.01	0.09	0.09	7.7	1.12	1.4	1.33
5	St	3.02	0.35	0.09	0.16	8.8	1.23	1.4	1.32
6	MMA	0.18	5.81	0.50	0.25	7.4	1.26	1.5	1.45

[a]The reactions were performed at 25 °C under nitrogen with an 18 W blue LED light (λ_{max} = 450 nm). $[M]_0$ = 0.5 M; $[EY]_0/[M]_0$ = 1000 ppm. [b]$F_1^{(end)}$ was determined by ^{1}H NMR spectroscopy. [c]M_n and $Đ$ were determined by SEC analysis calibrated to polystyrene standards.

Copolymerization of macrocyclic allylic sulfone and acrylic monomers. Encouraged by the homopolymerization results of **1**, we then investigated the copolymerization of **1** and acrylic monomers. First, **1** was copolymerized with *tert*-butyl acrylate (*t*BA) at [*t*BA]:[**1**]:[**CTA1**]=100:10:1, affording copolymer **P-1-*co*-*t*BA** with $M_n^{(SEC)}$ of 11.3 kg mol^{-1} and $Đ$ of 1.11 (Table 1, entry 1 and Figure 2A). The kinetic analysis of the copolymerization of **1** and *t*BA monitored by ^{1}H NMR revealed that both **1** and *t*BA followed first-order kinetics throughout the copolymerization (Figure 2B). Their observed rate constants were calculated for **1** and *t*BA to be k_1 = 0.44 h^{-1} and k_{tBA} = 0.43 h^{-1}, respectively. The molecular weight of **P-1-*co*-*t*BA** increased

linearly with the total conversion (*conv.*) of the two monomers (Figure 2C), which is defined by Equation (1) (Eq. 1):

$$conv. = 1 - \frac{[\mathbf{1}(t)]+[\mathbf{B}(t)]}{[\mathbf{1}(0)]+[\mathbf{B}(0)]} \quad (1)$$

where [**1**(t)] and [**B**(t)] are the instantaneous concentrations of **1** and vinyl monomer **B** at time *t,* respectively, and [**1**(0)] and [**B**(0)] are the initial concentrations of **1** and vinyl monomer **B**, respectively. The dispersity of **P-1-*co*-*t*BA** remained low throughout the copolymerization ($Đ$ < 1.2) (Figure 2C). These results indicated an excellent control throughout the copolymerization. By analyzing the ^{1}H NMR of the purified copolymers at different conversions, the molar fraction of **1** incorporated into the copolymer (denoted hereafter as $F_{\mathbf{1}}$) remained identical to the molar fraction of **1** in the initial comonomer mixture (denoted hereafter as $f_{\mathbf{1}}^0$) throughout the copolymerization ($F_{\mathbf{1}} = f_{\mathbf{1}}^0 = 0.09$) (Figure S2). These results suggested that the reactivities of **1** and *t*BA are similar during the organocatalyzed photocontrolled rROCCP. We used the reactivity ratios to quantitatively assess the reactivities of the two comonomers in the organocatalyzed photocontrolled rROCCP. To determine the reactivity ratios, the respective concentrations of **1** and *t*BA compared to the total conversions were fitted to the Beckingham-Sanoja-Lynd (BSL) integrated model, which is defined by Equations (2) and (3) (Eq. 2 and Eq. 3).[39-40]

$$conv. = 1 - f_{\mathbf{1}}^0 \left[\frac{\mathbf{1}(t)}{\mathbf{1}(0)}\right] - (1 - f_{\mathbf{1}}^0) \left[\frac{\mathbf{1}(t)}{\mathbf{1}(0)}\right]^{r_{\mathbf{B}}} \quad (2)$$

$$conv. = 1 - f_{\mathbf{1}}^0 \left[\frac{\mathbf{B}(t)}{\mathbf{B}(0)}\right]^{r_{\mathbf{1}}} - (1 - f_{\mathbf{1}}^0) \left[\frac{\mathbf{B}(t)}{\mathbf{B}(0)}\right] \quad (3)$$

The BSL integrated model is known to accurately determine the reactivity ratios of non-terminal copolymerization, where the rate of propagation completely depends on the reactivities of

monomers with minimal dependence on the propagating species. Independent fitting of the respective instantaneous concentrations of **1** and *t*BA at various *conv.* values to Eq. 2 and Eq. 3 yielded reactivity ratios of **1** and *t*BA as $r_{\mathbf{1}} = 1.04$ and $r_{t\mathrm{BA}} = 0.96$, respectively (Table 2, entry 1, Figure 2D, and Table S2). The product of the two independently derived reactivity ratios equals unity ($r_{\mathbf{1}} \times r_{t\mathrm{BA}} = 1.002$), suggesting that the BSL integrated model can be applied to this copolymerization system.[39-40] The close-to-unity reactivity ratios also suggest that the copolymerization of **1** and *t*BA formed random copolymers ($r_a = r_b = 1$) with the main-chain diester motif statistically incorporated in the copolymer backbone. The organocatalyzed photocontrolled rROCCP of **1** and *t*BA at other feed ratios ($f_{\mathbf{1}}^0 = 0.05$ and 0.25) afforded copolymers **P-1-*co*-*t*BA** with predictable $M_{\mathrm{n}}^{(\mathrm{SEC})}$ and low $Đ$ (Table 1, entry 2-4). Meanwhile, the $F_{\mathbf{1}}^{(\mathrm{end})}$ of the resulting copolymers all remained the same as their $f_{\mathbf{1}}^0$ (Table 1, entry 2-4). We further explored the copolymerization of **1** and other acrylic monomers, including MA, *N,N*-dimethylacrylamide (DMA), and *N*-Acryloylmorpholine (NAM). All these copolymerization exhibited excellent control over the polymerization and near-unity reactivity ratios ($r_{\mathbf{1}} = 1.02$ and $r_{\mathrm{MA}} = 0.98$; $r_{\mathbf{1}} = 0.98$ and $r_{\mathrm{DMA}} = 0.93$; $r_{\mathbf{1}} = 0.99$ and $r_{\mathrm{NAM}} = 1.01$), suggesting that the organocatalyzed photocontrolled rROCCP is generally applicable to acrylic monomers (Table 1, entry 5-12, Table 2, entry 2-4, Figure S3-S14, and Table S3-S5). To further confirm the statistical distribution of the degradable building block in the copolymer backbone, the copolymers were treated with sodium methoxide (NaOMe) to cleave the main-chain diester motif. Taking **P-1-*co*-*t*BA** as an example, after incubating with 25 wt% NaOMe in methanol at 25 ºC for 30 minutes, the $M_{\mathrm{n}}^{(\mathrm{SEC})}$ of the copolymer decreased from 10.6 kg mol^{-1} to 1.8 kg mol^{-1}, as evidenced by a clear shift of the original unimodal peak to the high elution time region on the SEC (Table 2, entry 1 and Figure 2E). Notably, the ^{1}H NMR analysis revealed that the methylene groups adjacent to the main-chain esters (3.78 to 4.22

ppm) disappeared, while the *tert*-butyl group stayed untouched (1.44 pm) after degradation (Figure S15). This result suggests that the ester linkages in the main chain of **P-1-*co*-*t*BA** were selectively cleaved, while the *tert*-butyl esters on the side chain remained intact. Furthermore, the degradation of **P-1-*co*-MA**, **P-1-*co*-DMA**, and **P-1-*co*-NAM** all exhibited a similarly dramatic molecular weight reduction (degraded $M_n^{(SEC)}$ < 1.5 kg mol^{-1}), suggesting the statistical incorporation of degradable units in the copolymer backbone (Table 2, entry 2-4 and Figure S16-S21).

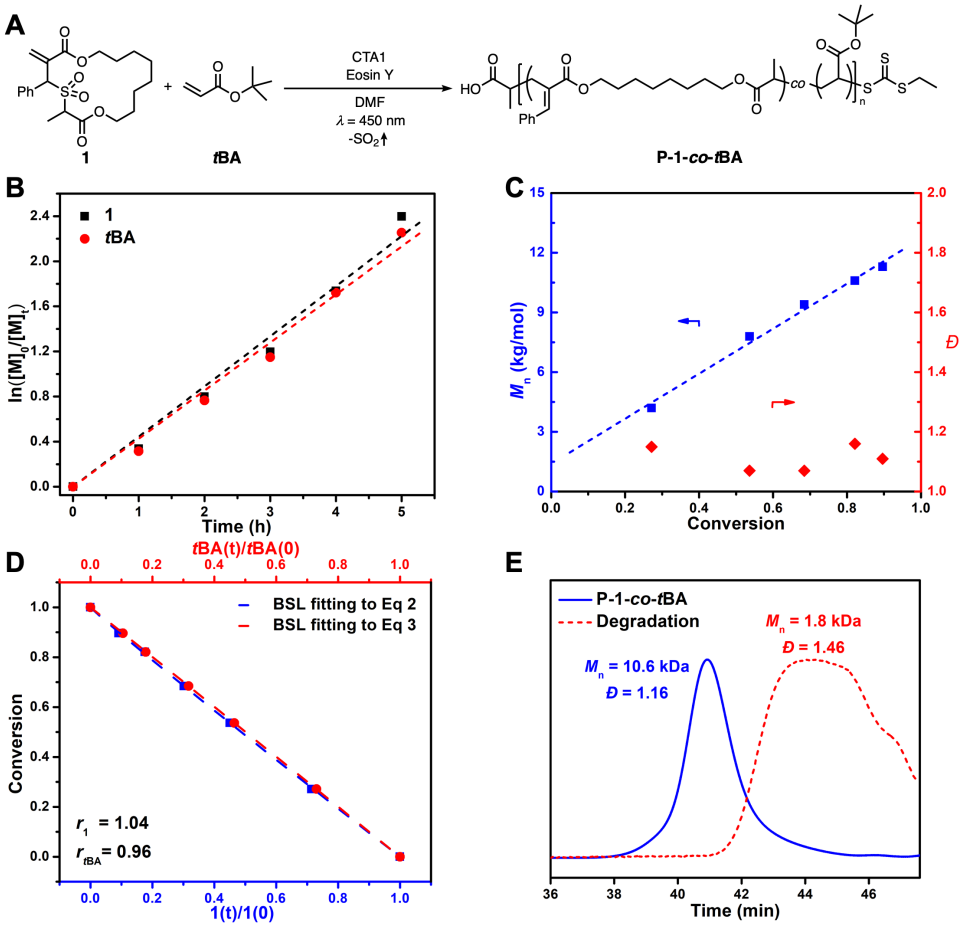

Figure 2. (A) Organocatalyzed photocontrolled rROCCP of **1** and *t*BA. (B) Kinetic plots of ln([M]$_0$/[M]$_t$) versus reaction time of **1** and *t*BA. (C) Plots of M_n and $Đ$ of **P-1-*co*-*t*BA** as a function of total conversion. (D) The plot of total conversion with respect to [**1**(t)]/[**1**(0)] and

[*t*BA(t)]/[*t*BA(0)] is fitted to Eq. 2 and Eq. 3 of the BSL integrated model independently to derive the reactivity ratios of **1** and *t*BA. (E) The degradation of **P-1-*co*-*t*BA** exhibited a clear shift of the copolymer peak to the low molecular weight region in SEC.

Copolymerization of macrocyclic allylic sulfone and styrene. With the global annual production of more than 16 million metric tons, polystyrene is one of the major sources of synthetic plastics, and new approaches to degradable polystyrene have attracted much attention.[21-22] We explored the organocatalyzed photocontrolled rROCCP of **1** and styrene (St) to incorporate degradable functionalities into the backbone of polystyrene. Regulated by Eosin Y and **CTA1** under $\lambda_{max} = 450$ nm blue light irradiation, the copolymerization of **1** and St at [St]:[**1**]:[**CTA1**]=100:10:1 yielded **P-1-*co*-St** with M_n^{SEC} of 8.8 kg mol^{-1} and $Đ$ of 1.23 (Table 1, entry 13 and Figure 3A). Degradable polystyrene with higher molecular weight (13.0 and 14.0 kg mol^{-1}) was also obtained when the $[M]_0/[I]_0$ ratios were increased (Table 1, entry 14-15). The kinetic study of the copolymerization of **1** and St monitored by ^{1}H NMR displayed first-order kinetics of both **1** and St, despite a slower rate of incorporation of St during the copolymerization ($k_{\mathbf{1}} = 0.030$ h^{-1} and $k_{St} = 0.011$ h^{-1}) (Figure 3B). The copolymerization of **1** and St also exhibited slower kinetics compared to the copolymerization of **1** and acrylic monomers, which is attributed to the lower reactivity of St than acrylic monomers and reduced catalyst efficiency caused by the triplet quenching of St.[38] Despite the lower rates, the M_n^{SEC} of **P-1-*co*-St** increased linearly with the total conversion of **1** and St, and low $Đ$ was maintained throughout the copolymerization (Figure 3C), indicating a well-controlled copolymerization. By fitting the instantaneous concentrations of **1** and St at various *conv.* values to the BSL integrated model, the reactivity ratios of **1** and St were determined as $r_{\mathbf{1}} = 3.02$ and $r_{St} = 0.35$, respectively (Table 2, entry 5, Figure 3D,

and Table S6). The product of the two independently derived reactivity ratios approximately equals to unity ($r_{\mathbf{1}} \times r_{\mathrm{St}} = 1.04$), supporting that the BSL integrated model is suitable to determine the reactivity ratios in the copolymerization of **1** and St. Higher incorporation of **1** (end-point copolymer composition $F_{\mathbf{1}}^{(\mathrm{end})} = 0.16$) in the copolymer than the feed composition ($f_{\mathbf{1}}^{0} = 0.09$) was confirmed by the ^{1}H NMR analysis of the purified **P-1-*co*-St** (Figure S22). The ^{1}H NMR analysis of the purified copolymers at different conversions also suggested that the ratio of degradable units incorporated into **P-1-*co*-St** decreased as the total conversion increased (Figure S22). The ^{1}H NMR analysis of the degraded **P-1-*co*-St** revealed successful cleavage of the main-chain ester groups in **P-1-*co*-St** (Figure S23). The SEC analysis of the degraded **P-1-*co*-St** also exhibited a dramatic molecular weight reduction (degraded $M_{\mathrm{n}}^{\mathrm{SEC}} = 1.4$ kg mol^{-1}, $Đ = 1.32$) (Table 2, entry 5 and Figure 3E), suggesting that the copolymer can be efficiently degraded.

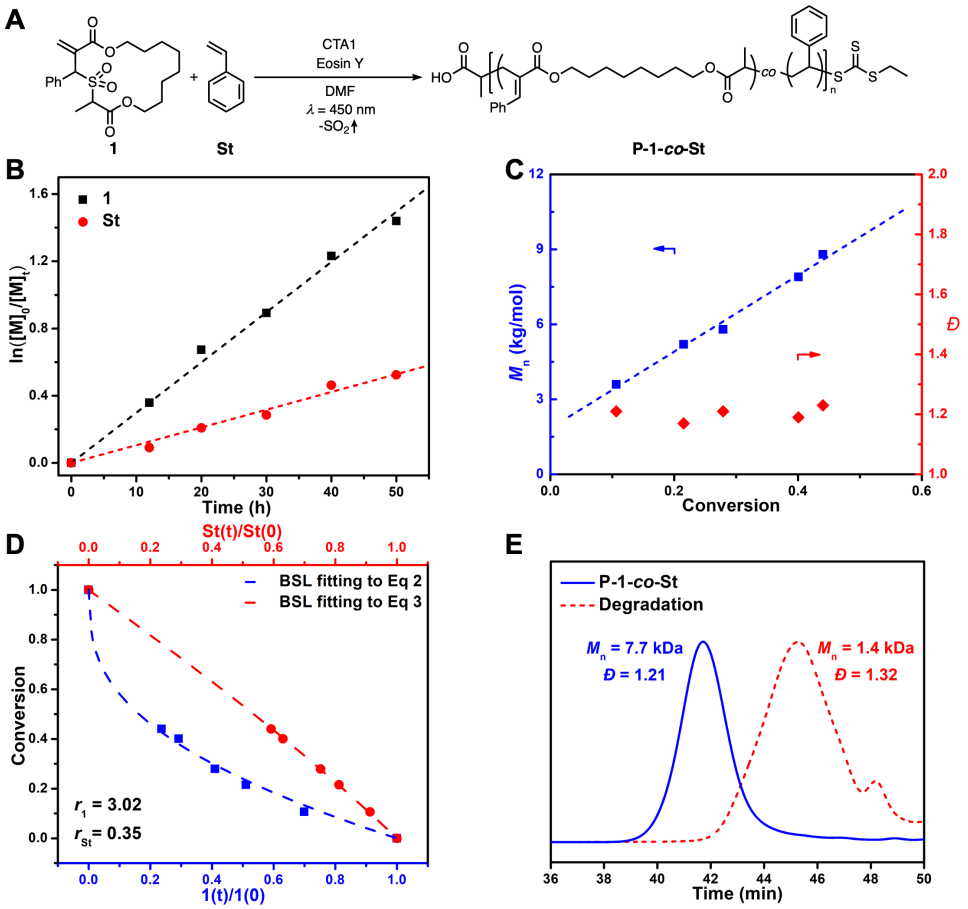

Figure 3. (A) Organocatalyzed photocontrolled rROCCP of **1** and St. (B) Kinetic plots of $\ln([M]_0/[M]_t)$ versus reaction time of **1** and St. (C) Plots of M_n and $Đ$ of **P-1-*co*-St** as a function of total conversion. (D) The plot of total conversion with respect to [**1**(t)]/[**1**(0)] and [St(t)]/[St(0)] is fitted to Eq. 2 and Eq. 3 of the BSL integrated model independently to derive the reactivity ratios of **1** and St. (E) Degradation of **P-1-*co*-St** exhibited a clear shift of the copolymer peak to the low molecular weight region in SEC.

Copolymerization of macrocyclic allylic sulfone and methyl methacrylate. We next turned our attention to the copolymerization of **1** and MMA. The initial attempt of the organocatalyzed photocontrolled rROCCP of **1** and MMA at [MMA]:[**1**]:[**CTA1**]=100:10:1 mediated by **CTA1** led

to the loss of control. A dithiobenzoate chain transfer agent **CTA2** with an enhanced addition rate and reduced fragmentation rate has been reported to facilitate better control over the homopolymerization of MMA.[41] Consistent with the previous report, the control over the copolymerization of **1** and MMA mediated by **CTA2** was improved, affording **P-1-*co*-MMA** with M_n^{SEC} of 11.5 kg mol^{-1} and $Đ$ of 1.36 (Table 1, entry 16 and Figure 4A). The kinetic analysis of the copolymerization of **1** and MMA showed that both **1** and MMA followed first-order kinetics (Figure 4B). Control over the polymerization was further confirmed by a linear increase of M_n^{SEC} of **P-1-*co*-MMA** with respect to the total conversion of **1** and MMA (Figure S24). However, the notably faster incorporation of MMA than **1** in the copolymerization ($k_{\mathbf{1}}$ = 0.006 h^{-1} and k_{MMA}= 0.033 h^{-1}) suggested that $F_{\mathbf{1}}$ was lower than $f_{\mathbf{1}}^0$. Indeed, ^{1}H NMR analysis of the purified copolymers revealed that less degradable main-chain diester motifs were incorporated in the backbone of **P-1-*co*-MMA** ($F_{\mathbf{1}}^{(end)}$ = 0.01) compared to its feed ratio ($f_{\mathbf{1}}^0$ = 0.09) (Table 1, entry 16 and Figure S25). The ^{1}H NMR analysis of the purified copolymers at different conversions also suggested that, contrary to **P-1-*co*-St**, the ratio of degradable units incorporated into **P-1-*co*-MMA** increased with the total conversion (Figure S25). Independently fitting the instantaneous concentrations of **1** and MMA of **P-1-*co*-MMA** at various *conv.* values to the BSL integrated model yielded the reactivity ratios of **1** and MMA $r_{\mathbf{1}}$ = 0.18 and r_{MMA} = 5.81, respectively (Table 2, entry 6, Figure 4C, and Table S7). The product of $r_{\mathbf{1}}$ and r_{MMA} equals to 1.04, suggesting that the BSL integrated model is suitable for determining the reactivity ratios in the copolymerization of **1** and MMA. The SEC analysis of the degradation of copolymer **P-1-*co*-MMA** with $F_{\mathbf{1}}^{(end)}$ = 0.01 only exhibited a moderate molecular weight reduction when treated with NaOMe, yielding oligomers with M_n^{SEC} of 7.2 kg mol^{-1} and $Đ$ of 1.29 (Figure 4D). The poor degradability is likely caused by the low incorporation of **1** in the copolymer. To improve the degradability of **P-1-*co*-**

MMA, f_1^0 was increased to 0.50, leading to an $F_1^{(end)}$ = 0.25 in the resulting copolymer (Table 1, entry 17). The degradability of the resulting **P-1-*co*-MMA** with $F_1^{(end)}$ = 0.25 was notably improved, producing fragments with lower molecular weight (degraded M_n^{SEC} = 1.5 kg mol^{-1}, $Đ$ = 1.45) after the NaOMe treatment (Table 2, entry 6 and Figure 4E).

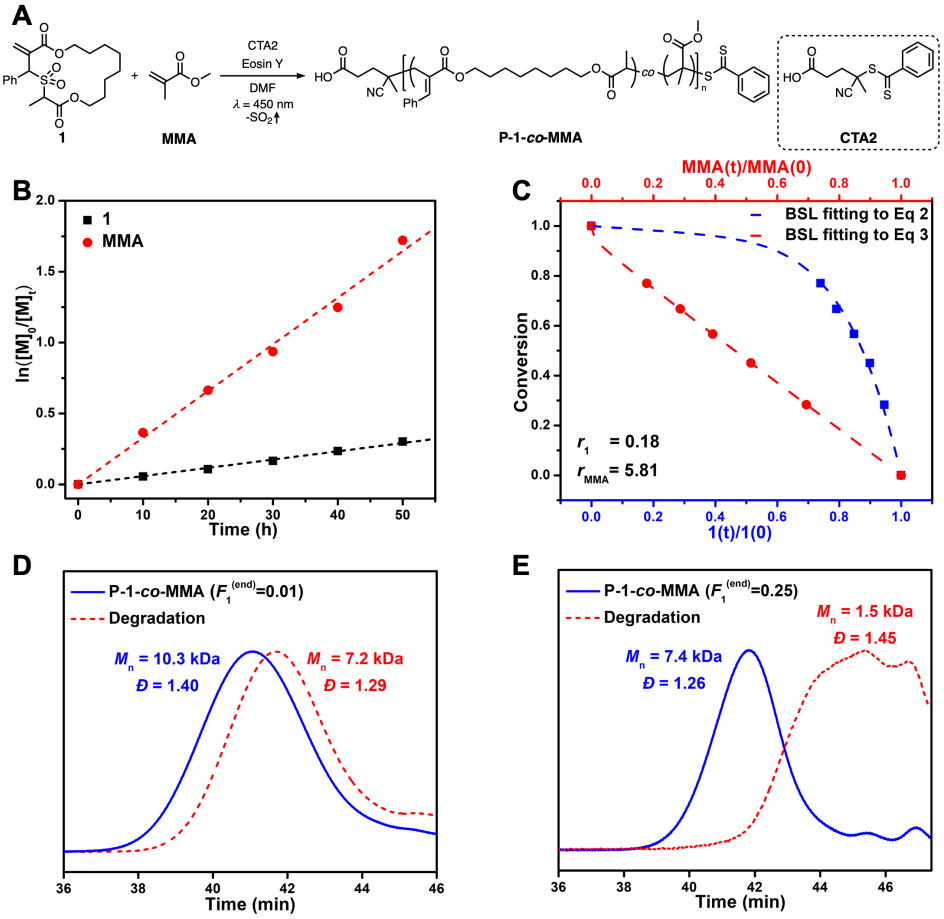

Figure 4. (A) Organocatalyzed photocontrolled rROCCP of **1** and MMA. (B) Kinetic plots of ln([M]$_0$/[M]$_t$) versus reaction time of **1** and MMA. (C) The plot of total conversion with respect to [**1**(t)]/[**1**(0)] and [MMA(t)]/[MMA(0)] is fitted to Eq. 2 and Eq. 3 of the BSL model independently to derive the reactivity ratios of **1** and MMA. (D) Degradation of **P-1-*co*-MMA** ($F_1^{(end)}$ = 0.01)

exhibited a moderate shift to the low molecular weight region in SEC. (E) Degradation of **P-1-*co*-MMA** ($F_1^{(end)}$ = 0.25) exhibited a clear shift to the low molecular weight region in SEC.

Thermal properties of the degradable vinyl copolymers. The thermal properties of the degradable vinyl copolymers were analyzed by thermogravimetry (TG) and differential scanning calorimetry (DSC). The TG analysis revealed that the 5% weight loss decomposition temperature (T_d) of **P-1-*co*-St** (T_d = 325-347 ºC when $F_1^{(end)}$ = 0.03-0.15) are higher than their corresponding homopolymers, T_d (polystyrene) = 307 ºC (Figure 5A). Similar results were also observed when **1** was copolymerized with MMA, where **P-1-*co*-MMA** (T_d = 275-313 ºC when $F_1^{(end)}$ = 0.01-0.25) demonstrated improved thermal stability compared to PMMA (T_d = 255 ºC) (Figure 5B). On the other hand, the glass transition temperatures (T_gs) of the degradable vinyl copolymers are dependent on the copolymer compositions. T_gs of **P-1-*co*-St** (T_g = 87 ºC when $F_1^{(end)}$ = 0.03, T_g = 73 ºC when $F_1^{(end)}$ = 0.04, T_g = 65 ºC when $F_1^{(end)}$ = 0.07, and T_g = 28 ºC when $F_1^{(end)}$ = 0.15) were reduced compared to the homopolymer, T_g (polystyrene) = 91 ºC, when more degradable units were incorporated into the copolymer backbone (Figure 5C). While T_g of **P-1-*co*-MMA** remains the same as the corresponding homopolymer when the composition of the degradable motif is low (T_g = 93 ºC when $F_1^{(end)}$ = 0.01), it decreases at a higher incorporation ratio of the degradable motif (T_g = 44 ºC when $F_1^{(end)}$ = 0.04, T_g = 38 ºC when $F_1^{(end)}$ = 0.11, and T_g = 19 ºC when $F_1^{(end)}$ = 0.25) (Figure 5D). The higher T_d and lower T_g values of the degradable vinyl copolymers can both be attributed to the incorporation of the main-chain diester motif from **1**, which has high thermal stability and contains a flexible octanediol spacer that reduces the rigidity of the copolymer chains. Therefore, the thermal properties of the copolymers are readily tunable by the incorporation of the degradable motif.

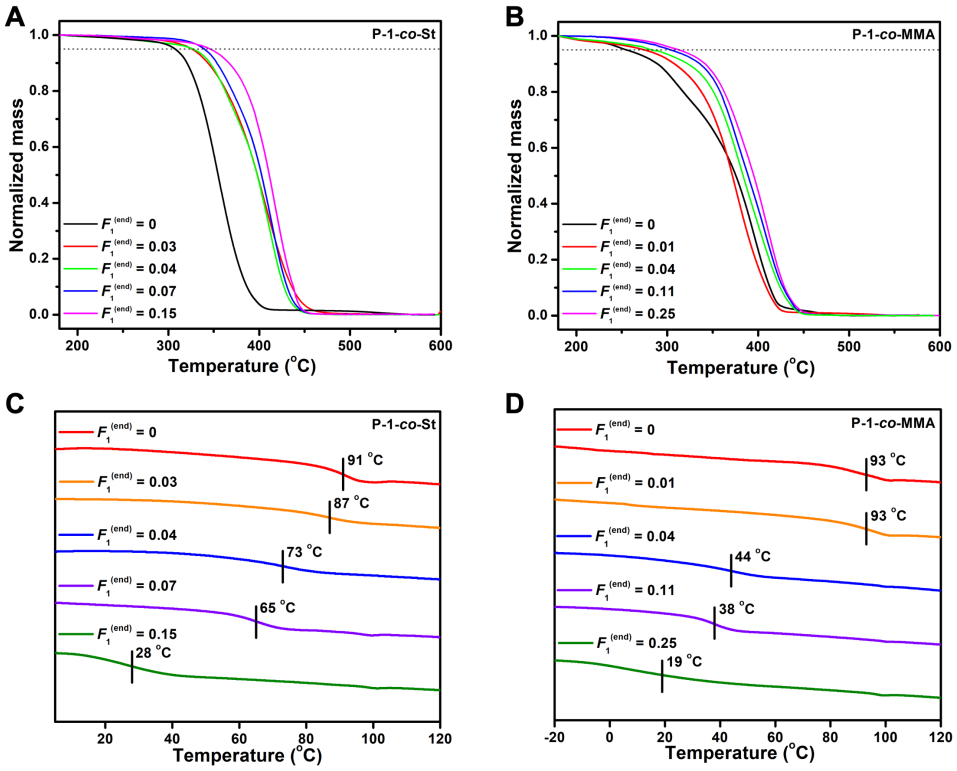

Figure 5. Thermal properties of the degradable vinyl copolymers in comparison to their corresponding homopolymers. (A) T_d of polystyrene and **P-1-*co*-St** at $F_1^{(end)}$ = 0.03, 0.04, 0.07, and 0.15. (B) T_d of PMMA and **P-1-*co*-MMA** at $F_1^{(end)}$ = 0.01, 0.04, 0.11, and 0.25. (C) T_g of polystyrene and **P-1-*co*-St** at $F_1^{(end)}$ = 0.03, 0.04, 0.07, and 0.15. (D) T_g of PMMA and **P-1-*co*-MMA** at $F_1^{(end)}$ = 0.01, 0.04, 0.11, and 0.25.

CONCLUSION

In summary, this work demonstrated that macrocyclic allylic sulfone can serve as a universal comonomer to copolymerize with various conjugated vinyl monomers, including acrylates,

acrylamides, styrene, and methacrylate, in the organocatalyzed photocontrolled radical ring-opening cascade copolymerization. Fitting the copolymer compositions to the Beckingham-Sanoya-Lynd integrated model revealed unity reactivity ratios in the copolymerization of macrocyclic allylic sulfone and acrylic monomers. While macrocyclic allylic sulfone exhibited similar reactivity to acrylates and acrylamides in copolymerization, its incorporation rate is higher than styrene but lower than methyl methacrylate. As a result, a higher initial feed composition of the macrocyclic allylic sulfone is required to achieve appreciable incorporation in the copolymerization with methyl methacrylate. The approach described in this article represents a powerful method to incorporate degradability into mass-produced commodity vinyl plastics. Moving forward, improvement of the reactivity of macrocyclic allylic sulfone in the copolymerization with various vinyl monomers may benefit from further optimization of the macrocyclic allylic sulfone structure and reaction conditions (e.g., solvent, temperature, and method of initiation).

ASSOCIATED CONTENT

Supporting Information

The Supporting Information is available free of charge on the ACS Publications website.

AUTHOR INFORMATION

Corresponding Author

Jia Niu - Department of Chemistry, Boston College, Chestnut Hill, Massachusetts 02467, United States; orcid.org/0000-0002-5622-6362; E-mail: jia.niu@bc.edu

Authors

Wenqi Wang - Department of Chemistry, Boston College, Chestnut Hill, Massachusetts 02467, United States

Brayan Rondon - Department of Chemistry, Boston College, Chestnut Hill, Massachusetts 02467, United States

Zeyu Wang - School of Polymer Science and Polymer Engineering, the University of Akron, Akron, Ohio 44325, United States; orcid.org/0000-0002-6343-0548

Junpeng Wang - School of Polymer Science and Polymer Engineering, the University of Akron, Akron, Ohio 44325, United States; orcid.org/0000-0002-4503-5026

Notes

The authors declare no competing financial interest.

ACKNOWLEDGMENTS

This research is primarily supported by an NSF CAREER award (CHE-1944512) to J.N. Financial support is also provided by an ACS PRF Doctoral New Investigator Award (60747DNI7) to J.N. The NMR characterization of this research is supported by an NSF MRI award (CHE2117246) and an NIH HEI-S10 award (1S10OD026910-01A1).

REFERENCES

1. Geyer, R.; Jambeck, J. R.; Law, K. L. Production, use, and fate of all plastics ever made. *Sci. Adv*. **2017**, *3*, e1700782.
2. Chamas, A.; Moon, H.; Zheng, J.; Qiu, Y.; Tabassum, T.; Jang, J. H.; Abu-Omar, M.; Scott, S. L.; Suh, S. Degradation Rates of Plastics in the Environment. *ACS Sustainable Chem. Eng*. **2020**, *8*, 3494-3511.

3. Seeley, M. E.; Song, B.; Passie, R.; Hale, R. C. Microplastics affect sedimentary microbial communities and nitrogen cycling. *Nat. Commun*. **2020**, *11*, 2372.
4. Kakadellis, S.; Rosetto, G. Achieving a circular bioeconomy for plastics. *Science* **2021**, *373*, 49-50.
5. MacLeod, M.; Arp, H. P. H.; Tekman, M. B.; Jahnke, A. The global threat from plastic pollution. *Science* **2021**, *373*, 61-65.
6. Korley, L. T. J.; Epps, T. H.; Helms, B. A.; Ryan, A. J. Toward polymer upcycling-adding value and tackling circularity. *Science* **2021**, *373*, 66-69.
7. Errede, L. A. The Chemistry of Xylylenes. X. Some Polymers and Telomers of *Spiro*-di-*o*-xylylene. *J. Polym. Sci*. **1961**, *49*, 253-265.
8. Bailey, W. J. Free Radical Ring-Opening Polymerization. *Polym. J*. **1985**, *17*, 85-95.
9. Delplace, V.; Nicolas, J. Degradable vinyl polymers for biomedical applications. *Nat. Chem*. **2015**, *7*, 771-784.
10. Tardy, A.; Nicolas, J.; Gigmes, D.; Lefay, C.; Guillaneuf, Y. Radical Ring-Opening Polymerization: Scope, Limitations, and Application to (Bio)Degradable Materials. *Chem. Rev*. **2017**, *117*, 1319-1406.
11. Pesenti, T.; Nicolas, J. 100th Anniversary of Macromolecular Science Viewpoint: Degradable Polymers from Radical Ring-Opening Polymerization: Latest Advances, New Directions, and Ongoing Challenges. *ACS Macro Lett.* **2020**, *9*, 1812-1835.
12. Bailey, W. J.; Ni, Z.; Wu, S.-R. Synthesis of Poly-ϵ-Caprolactone via a Free Radical Mechanism. Free Radical Ring-Opening Polymerization of 2-Methylene-1,3-Dioxepane. *J. Polym. Sci., Polym. Chem. Ed*. **1982**, *20*, 3021-3030.

13. Endo, T.; Okawara, M.; Bailey, W. J.; Azuma, K.; Nate, K.; Yokono, H. Photoinitiated Ring-Opening Polymerization of 2-Methylene-1,3-Dioxepane. *J. Polym. Sci., Polym. Lett. Ed.* **1983**, *21*, 373-380.
14. Hedir, G. G.; Bell, C. A.; Ieong, N. S.; Chapman, E.; Collins, I. R.; O'Reilly, R. K.; Dove, A. P. Functional Degradable Polymers by Xanthate-Mediated Polymerization. *Macromolecules* **2014**, *47*, 2847-2852.
15. Delplace, V.; Guégain, E.; Harrisson, S.; Gigmes, D.; Guillaneuf, Y.; Nicolas, J. A ring to rule them all: a cyclic ketene acetal comonomer controls the nitroxide-mediated polymerization of methacrylates and confers tunable degradability. *Chem. Commun*. **2015**, *51*, 12847-12850.
16. Hill, M. R.; Guégain, E.; Tran, J.; Figg, C. A.; Turner, A. C.; Nicolas, J.; Sumerlin, B. S. Radical Ring-Opening Copolymerization of Cyclic Ketene Acetals and Maleimides Affords Homogeneous Incorporation of Degradable Units. *ACS Macro Lett.* **2017**, *6*, 1071-1077.
17. Tardy, A.; Honoré, J.-C.; Tran, J.; Siri, D.; Delplace, V.; Bataille, I.; Letourneur, D.; Perrier, J.; Nicoletti, C.; Maresca, M.; Lefay, C.; Gigmes, D.; Nicolas, J.; Guillaneuf, Y. Radical Copolymerization of Vinyl Ethers and Cyclic Ketene Acetals as a Versatile Platform to Design Functional Polyesters. *Angew. Chem., Int. Ed.* **2017**, *56*, 16515-16520.
18. Bingham, N. M.; Roth, P. J. Degradable vinyl copolymers through thiocarbonyl addition-ring-opening (TARO) polymerization. *Chem. Commun*. **2019**, *55*, 55-58.
19. Smith, R. A.; Fu, G.; McAteer, O.; Xu, M.; Gutekunst, W. R. Radical Approach to Thioester-Containing Polymers. *J. Am. Chem. Soc*. **2019**, *141*, 1446-1451.

20. Spick, M. P.; Bingham, N. M.; Li, Y.; de Jesus, J.; Costa, C.; Bailey, M. J.; Roth, P. J. Fully Degradable Thioester-Functional Homo- and Alternating Copolymers Prepared through Thiocarbonyl Addition-Ring-Opening RAFT Radical Polymerization. *Macromolecules* **2020**, *53*, 539-547.
21. Kiel, G. R.; Lundberg, D. J.; Prince, E.; Husted, K. E. L.; Johnson, A. M.; Lensch, V.; Li, S.; Shieh, P.; Johnson, J. A. Cleavable Comonomers for Chemically Recyclable Polystyrene: A General Approach to Vinyl Polymer Circularity. *J. Am. Chem. Soc*. **2022**, *144*, 12979-12988.
22. Gil, N.; Caron, B.; Siri, D.; Roche, J.; Hadiouch, S.; Khedaioui, D.; Ranque, S.; Cassagne, C.; Montarnal, D.; Gigmes, D.; Lefay, C.; Guillaneuf, Y. Degradable Polystyrene via the Cleavable Comonomer Approach. *Macromolecules* **2022**, *55*, 6680-6694.
23. Elliss, H.; Dawson, F.; Nisa, Q. u.; Bingham, N. M.; Roth, P. J.; Kopeć, M. Fully Degradable Polyacrylate Networks from Conventional Radical Polymerization Enabled by Thionolactone Addition. *Macromolecules*, **2022**, *55*, 6695-6702.
24. Nisa, Q. u.; Theobald, W.; Hepburn, K. S.; Riddlestone, I.; Bingham, N. M.; Kopeć, M.; Roth, P. J. Degradable Linear and Bottlebrush Thioester-Functional Copolymers through Atom-Transfer Radical Ring-Opening Copolymerization of a Thionolactone. *Macromolecules* **2022**, *55*, 7392-7400.
25. Chen, M.; Zhong, M.; Johnson, J. A. Light-Controlled Radical Polymerization: Mechanisms, Methods, and Applications. *Chem. Rev.* **2016**, *116*, 10167-10211.
26. Lai, H.; Zhang, J.; Xing, F.; Xiao, P. Recent advances in light-regulated non-radical polymerisations. *Chem. Soc. Rev.* **2020**, *49*, 1867-1886.

27. Wu, C.; Corrigan, N.; Lim, C.-H.; Liu, W.; Miyake, G.; Boyer, C. Rational Design of Photocatalysts for Controlled Polymerization: Effect of Structures on Photocatalytic Activities. *Chem. Rev*. **2022**, *122*, 5476-5518.
28. Parkatzidis, K.; Wang, H. S.; Truong, N. P.; Anastasaki, A. Recent Developments and Future Challenges in Controlled Radical Polymerization: A 2020 Update. *Chem*. **2020**, *6*, 1575-1588.
29. Corrigan, N.; Jung, K.; Moad, G.; Hawker, C. J.; Matyjaszewski, K.; Boyer, C. Reversible-deactivation radical polymerization (Controlled/living radical polymerization): From discovery to materials design and applications. *Prog. Polym. Sci*. **2020**, *111*, 101311.
30. Truong, N. P.; Jones, G. R.; Bradford, K. G. E.; Konkolewicz, D.; Anastasaki, A. A comparison of RAFT and ATRP methods for controlled radical polymerization. *Nat. Rev. Chem*. **2021**, *5*, 859-869.
31. Li, N.; Ding, D.; Pan, X.; Zhang, Z.; Zhu, J.; Boyer, C.; Zhu, X. Temperature programed photo-induced RAFT polymerization of stereo-block copolymers of poly(vinyl acetate). *Polym. Chem*. **2017**, *8*, 6024-6027.
32. Chen, D.-F.; Boyle, B. M.; McCarthy, B. G.; Lim, C.-H.; Miyake, G. M. Controlling Polymer Composition in Organocatalyzed Photoredox Radical Ring-Opening Polymerization of Vinylcyclopropanes. *J. Am. Chem. Soc*. **2019**, *141*, 13268-13277.
33. Wang, W.; Zhou, Z.; Sathe, D.; Tang, X.; Moran, S.; Jin, J.; Haeffner, F.; Wang, J.; Niu, J. Degradable Vinyl Random Copolymers via Photocontrolled Radical Ring-Opening Cascade Copolymerization. *Angew. Chem., Int. Ed.* **2022**, *61*, e202113302.

34. Treat, N. J.; Sprafke, H.; Kramer, J. W.; Clark, P. G.; Barton, B. E.; Read de Alaniz, J.; Fors, B. P.; Hawker, C. J. Metal-Free Atom Transfer Radical Polymerization. *J. Am. Chem. Soc*. **2014**, *136*, 16096-16101.

35. Miyake, G. M.; Theriot, J. C. Perylene as an Organic Photocatalyst for the Radical Polymerization of Functionalized Vinyl Monomers through Oxidative Quenching with Alkyl Bromides and Visible Light. *Macromolecules* **2014**, *47*, 8255-8261.

36. Xu, J.; Shanmugam, S.; Duong, H. T.; Boyer, C. Organo-photocatalysts for photoinduced electron transfer-reversible addition-fragmentation chain transfer (PET-RAFT) polymerization. *Polym. Chem*. **2015**, *6*, 5615-5624.

37. Theriot, J. C.; Lim, C.-H.; Yang, H.; Ryan, M. D.; Musgrave, C. B.; Miyake, G. M. Organocatalyzed atom transfer radical polymerization driven by visible light. *Science* **2016**, *352*, 1082-1086.

38. Corbin, D. A.; Miyake, G. M. Photoinduced Organocatalyzed Atom Transfer Radical Polymerization (O-ATRP): Precision Polymer Synthesis Using Organic Photoredox Catalysis. *Chem. Rev*. **2022**, *122*, 1830-1874.

39. Beckingham, B. S.; Sanoja, G. E.; Lynd, N. A. Simple and Accurate Determination of Reactivity Ratios Using a Nonterminal Model of Chain Copolymerization. *Macromolecules* **2015**, *48*, 6922-6930.

40. Lynd, N. A.; Ferrier, R. C.; Beckingham, B. S. Recommendation for Accurate Experimental Determination of Reactivity Ratios in Chain Copolymerization. *Macromolecules* **2019**, *52*, 2277-2285.

41. Perrier, S. 50th Anniversary Perspective: RAFT Polymerization-A User Guide. *Macromolecules* **2017**, *50*, 7433-7447.

Supporting Information

Macrocyclic Allylic Sulfone as A Universal Comonomer in Organocatalyzed Photocontrolled Radical Copolymerization with Vinyl Monomers

Wenqi Wang,[1] Brayan Rondon,[1] Zeyu Wang,[2] Junpeng Wang,[2] and Jia Niu*[1]

[1]Department of Chemistry, Boston College, Chestnut Hill, Massachusetts 02467, United States

[2]School of Polymer Science and Polymer Engineering, the University of Akron, Akron, Ohio 44325, United States

Correspondence to: jia.niu@bc.edu

Supplementary Results

Table S1. The screening of photocatalyst loading and initial monomer concentration for the organocatalyzed photoredox radical homopolymerization of **1**.

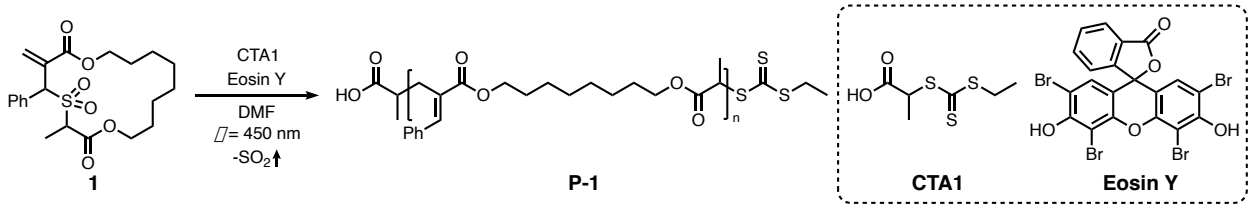

Entry[a]	$[EY]_0/[M]_0$	$[M]_0$	Conversion[b]	$M_n^{(SEC)}$ (kg mol^{-1})[c]	$Đ$[c]
1	200 ppm	0.2 M	20 %	3.0	1.08
2	500 ppm	0.2 M	56 %	6.6	1.26
3	1000 ppm	0.2 M	69 %	7.2	1.37
4	1500 ppm	0.2 M	68 %	7.4	1.37
5[d]	1000 ppm	0.5 M	68 %	7.7	1.13

[a]The reactions were performed at 25 °C under nitrogen with an 18 W blue LED light (λ_{max} = 450 nm) for 10 hours. [b]Monomer conversion was determined by ^{1}H NMR spectroscopy. [c]M_n and $Đ$ were determined by SEC analysis calibrated to polystyrene standards. [d]Reaction time: 4 hours.

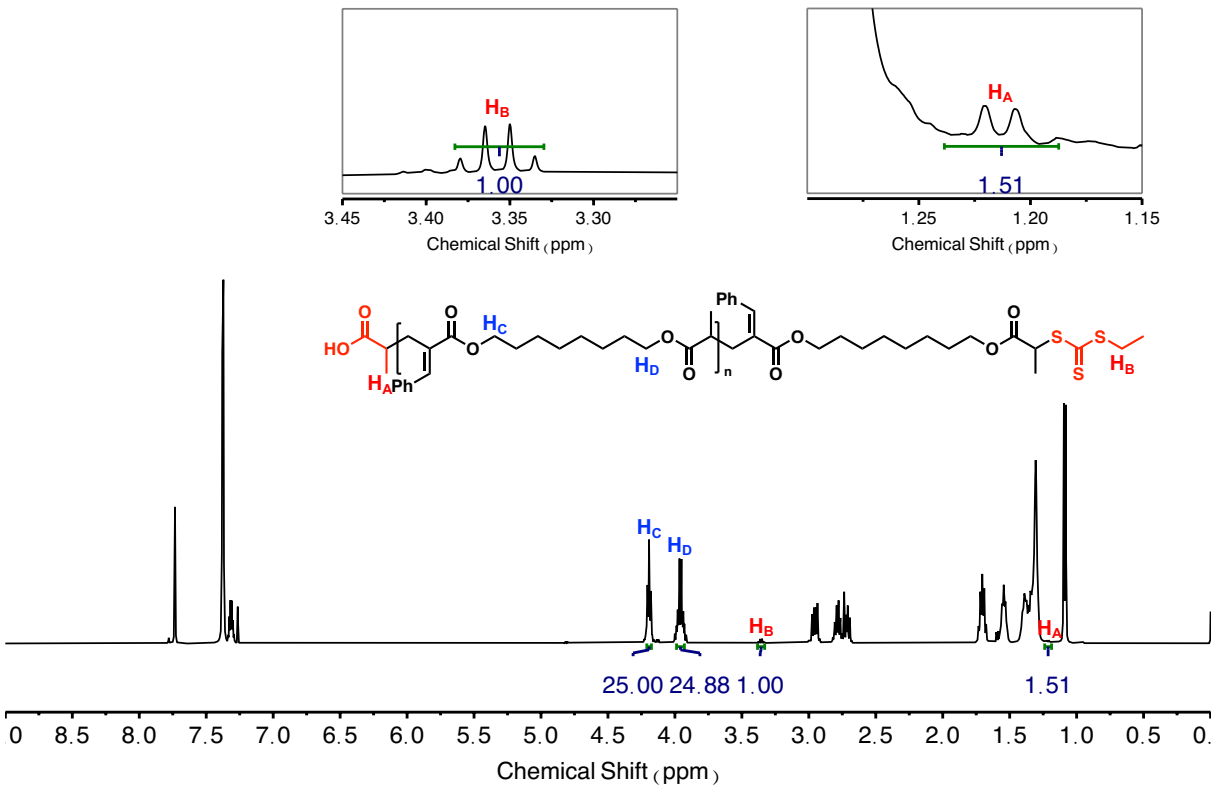

Figure S1. ^{1}H NMR spectroscopy of **P-1-8k**.

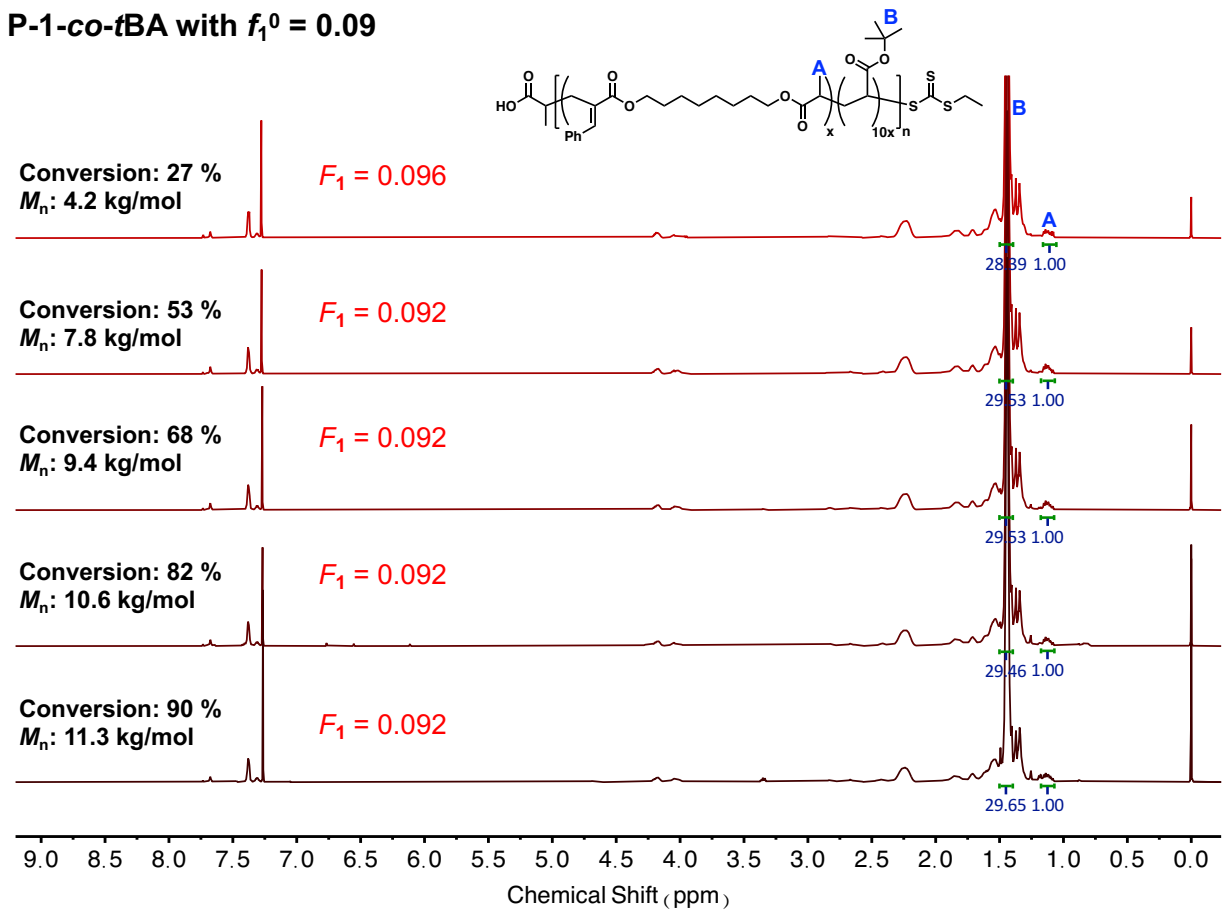

Figure S2. Compositional analysis of **P-1-*co*-*t*BA** at f_1^0 = 0.09 at different time points of the copolymerization by ^{1}H NMR. The incorporation of **1** in **P-1-*co*-*t*BA** (F_1) was determined by the following equation:

$$F_1 = \frac{3 \times I_A}{3 \times I_A + I_B}$$

Table S2. The summary of copolymerization results of **1** and *t*BA at f_1^0 = 0.09 at different time points.

Time (h)	**1**(t)/**1**(0)	*t*BA(t)/*t*BA(0)	*conv.*
1	0.72	0.73	0.27
2	0.45	0.47	0.54
3	0.30	0.32	0.68
4	0.18	0.18	0.82
5	0.09	0.11	0.90

The reactivity ratios of **1** and *t*BA were derived through a nonlinear fitting of the respective instantaneous concentrations of **1** and *t*BA at various *conv.* values to Eq. 2 and Eq. 3 independently.

$$conv. = 1 - f_{\mathbf{1}}^0 \left[\frac{\mathbf{1}(t)}{\mathbf{1}(0)}\right] - (1 - f_{\mathbf{1}}^0) \left[\frac{\mathbf{1}(t)}{\mathbf{1}(0)}\right]^{r_{t\mathrm{BA}}} \quad (2)$$

$$conv. = 1 - f_{\mathbf{1}}^0 \left[\frac{t\mathrm{BA}(t)}{t\mathrm{BA}(0)}\right]^{r_{\mathbf{1}}} - (1 - f_{\mathbf{1}}^0) \left[\frac{t\mathrm{BA}(t)}{t\mathrm{BA}(0)}\right] \quad (3)$$

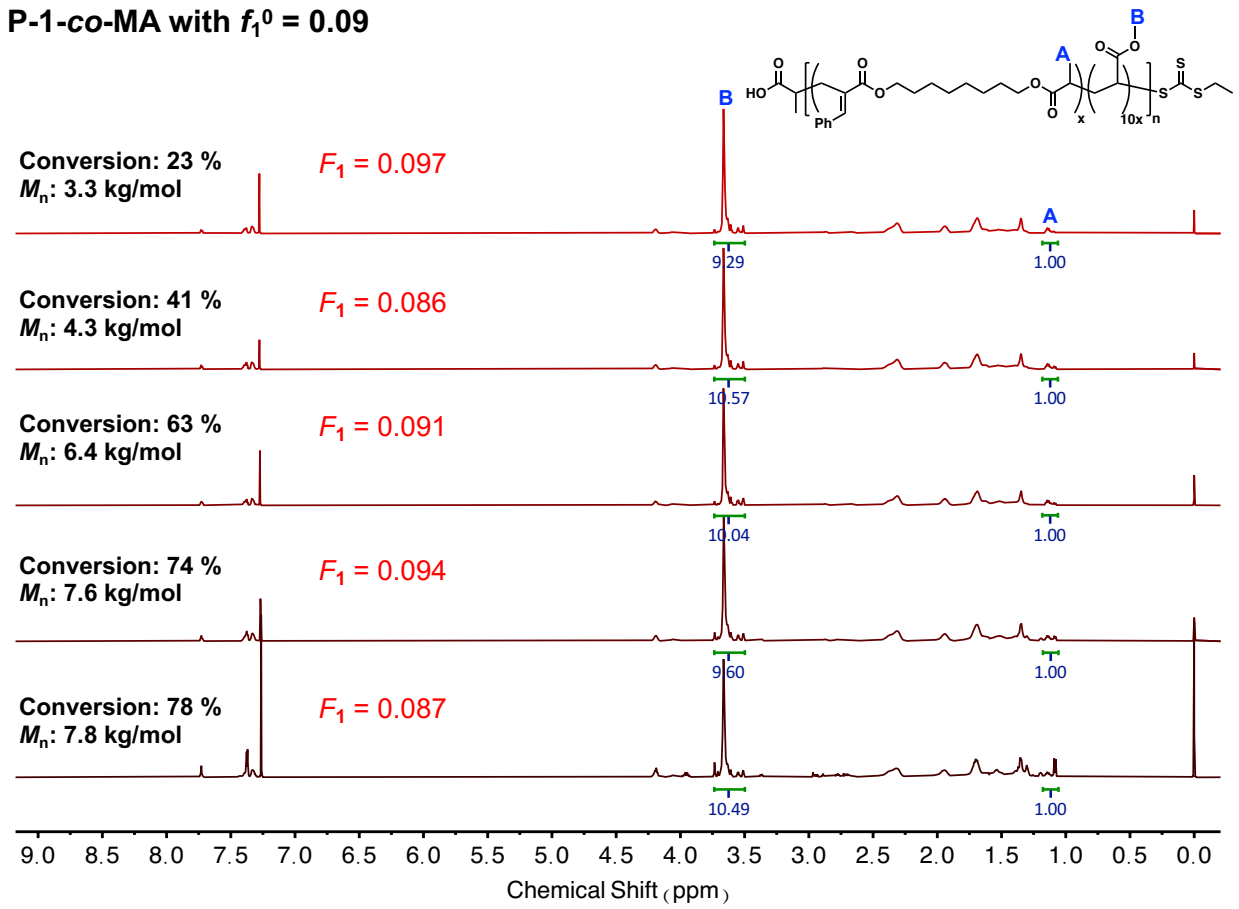

Figure S3. Compositional analysis of **P-1-*co*-MA** at f_1^0 = 0.09 at different time points of the copolymerization by ^{1}H NMR. The incorporation of **1** in **P-1-*co*-MA** (F_1) was determined by the following equation:

$$F_1 = \frac{I_A}{I_A + I_B}$$

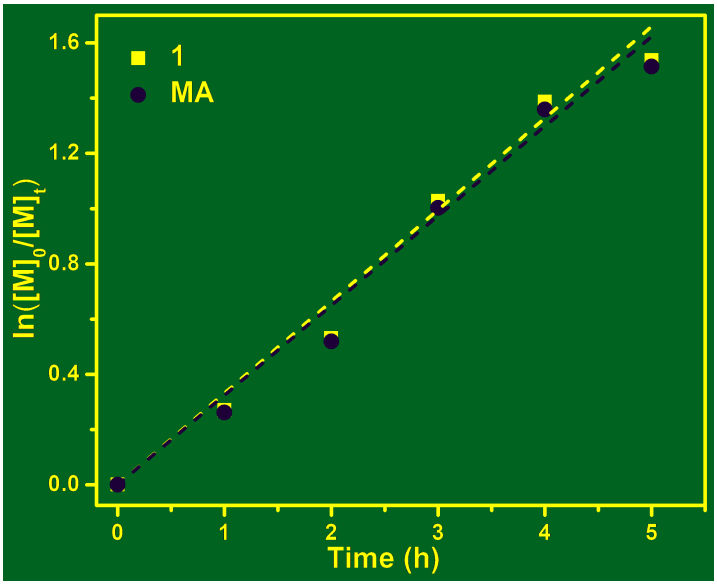

Figure S4. Kinetic plots of the organocatalyzed photocontrolled radical ring-opening cascade copolymerization of **1** and MA at $f_1^0 = 0.09$.

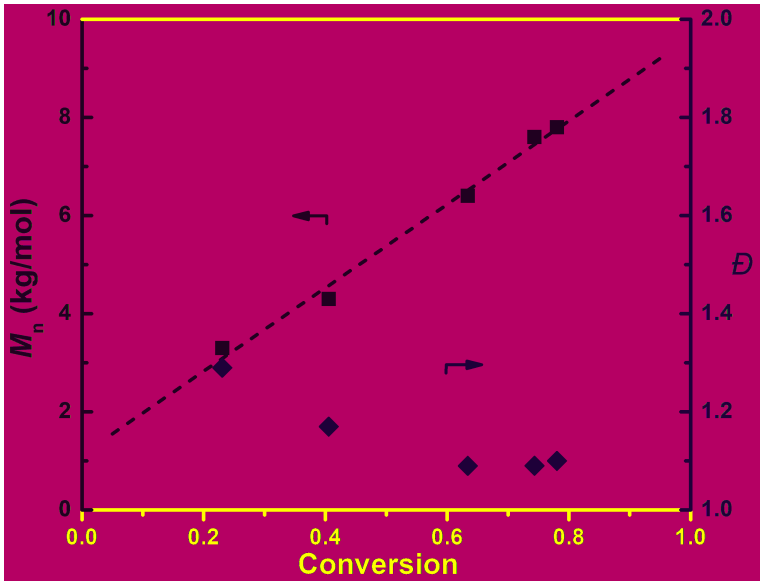

Figure S5. Plots of M_n and $Đ$ of **P-1-*co*-MA** as a function of total conversion.

Table S3. The summary of copolymerization results of **1** and MA at $f_{\mathbf{1}}^{0}$ = 0.09 at different time points.

Time (h)	**1**(t)/**1**(0)	MA(t)/MA(0)	*conv.*
1	0.76	0.77	0.23
2	0.59	0.60	0.41
3	0.36	0.37	0.63
4	0.25	0.26	0.74
5	0.22	0.22	0.78

The reactivity ratios of **1** and MA were derived through a nonlinear fitting of the respective instantaneous concentrations of **1** and MA at various *conv.* values to Eq. 2 and Eq. 3 independently.

$$conv. = 1 - f_{\mathbf{1}}^{0}\left[\frac{\mathbf{1}(t)}{\mathbf{1}(0)}\right] - (1 - f_{\mathbf{1}}^{0})\left[\frac{\mathbf{1}(t)}{\mathbf{1}(0)}\right]^{r_{\mathrm{MA}}} \quad (2)$$

$$conv. = 1 - f_{\mathbf{1}}^{0}\left[\frac{\mathrm{MA}(t)}{\mathrm{MA}(0)}\right]^{r_{\mathbf{1}}} - (1 - f_{\mathbf{1}}^{0})\left[\frac{\mathrm{MA}(t)}{\mathrm{MA}(0)}\right] \quad (3)$$

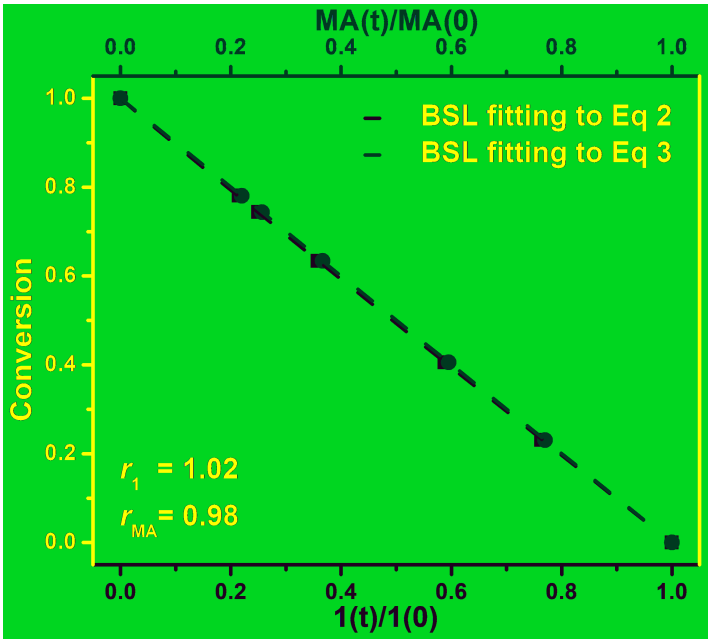

Figure S6. The plot of total conversion with respect to [**1**(t)]/[**1**(0)] and [MA(t)]/[MA(0)] is fitted to Eq. 2 and Eq. 3 of the BSL integrated model independently to derive the comonomer reactivity ratios for the copolymerization of **1** and MA at $f_1^0 = 0.09$.

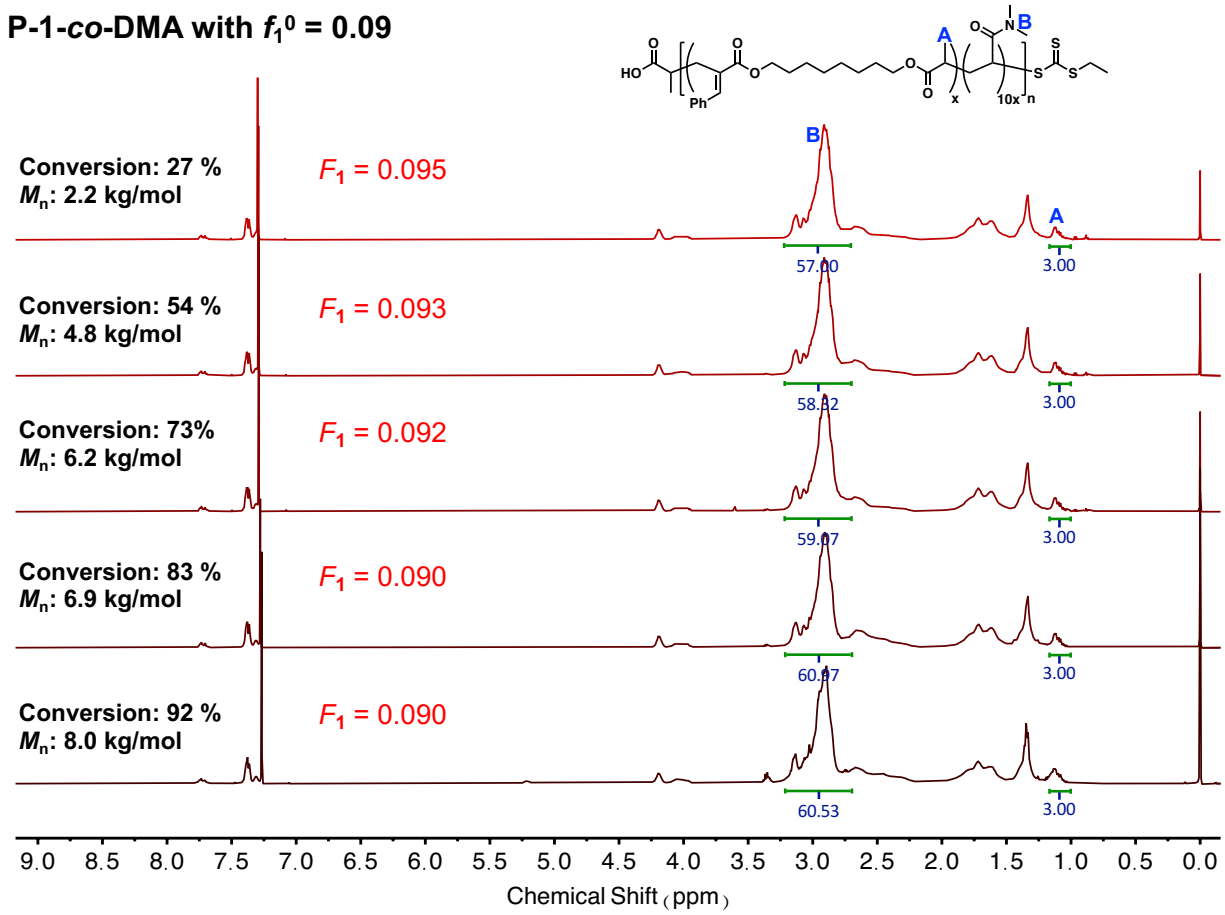

Figure S7. Compositional analysis of **P-1-*co*-DMA** at f_1^0 = 0.09 at different time points of the copolymerization by ^{1}H NMR. The incorporation of **1** in **P-1-*co*-DMA** (F_1) was determined by the following equation:

$$F_1 = \frac{2 \times I_A}{2 \times I_A + I_B}$$

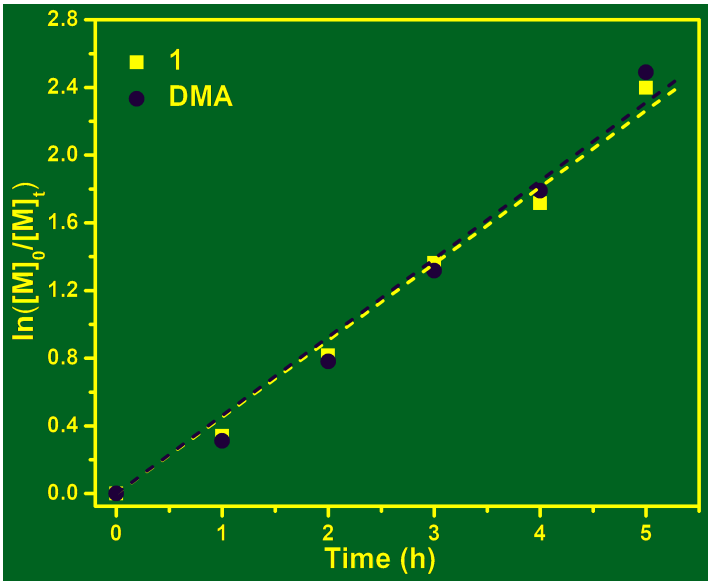

Figure S8. Kinetic Plots of the organocatalyzed photocontrolled radical ring-opening cascade copolymerization of **1** and DMA at $f_1^0 = 0.09$.

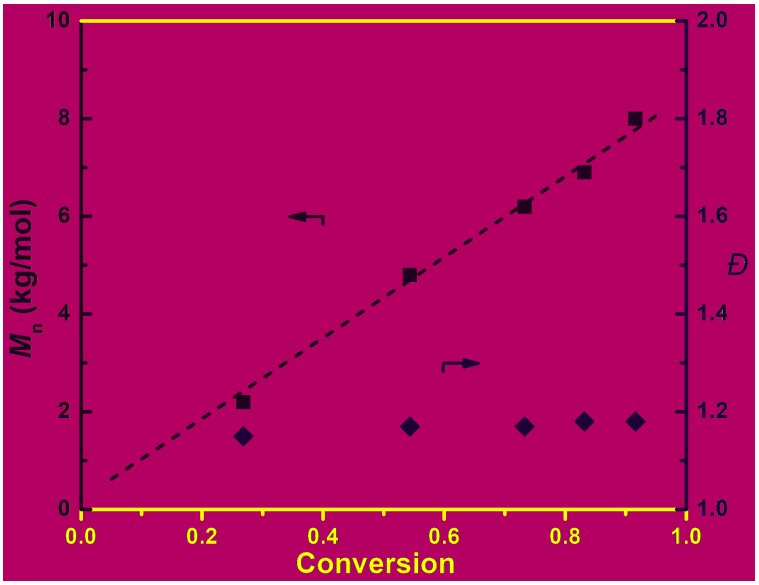

Figure S9. Plots of M_n and $Đ$ of **P-1-*co*-DMA** as a function of total conversion.

Table S4. The summary of copolymerization results of **1** and DMA at $f_1^0 = 0.09$ at different time points.

Time (h)	**1**(t)/**1**(0)	DMA(t)/DMA(0)	*conv.*
1	0.72	0.73	0.27
2	0.44	0.46	0.54
3	0.26	0.27	0.73
4	0.18	0.17	0.83
5	0.09	0.08	0.92

The reactivity ratios of **1** and DMA were derived through a nonlinear fitting of the respective instantaneous concentrations of **1** and DMA at various *conv.* values to Eq. 2 and Eq. 3 independently.

$$conv. = 1 - f_1^0 \left[\frac{\mathbf{1}(t)}{\mathbf{1}(0)}\right] - (1 - f_1^0) \left[\frac{\mathbf{1}(t)}{\mathbf{1}(0)}\right]^{r_{\mathrm{DMA}}} \quad (2)$$

$$conv. = 1 - f_1^0 \left[\frac{\mathrm{DMA}(t)}{\mathrm{DMA}(0)}\right]^{r_1} - (1 - f_1^0) \left[\frac{\mathrm{DMA}(t)}{\mathrm{DMA}(0)}\right] \quad (3)$$

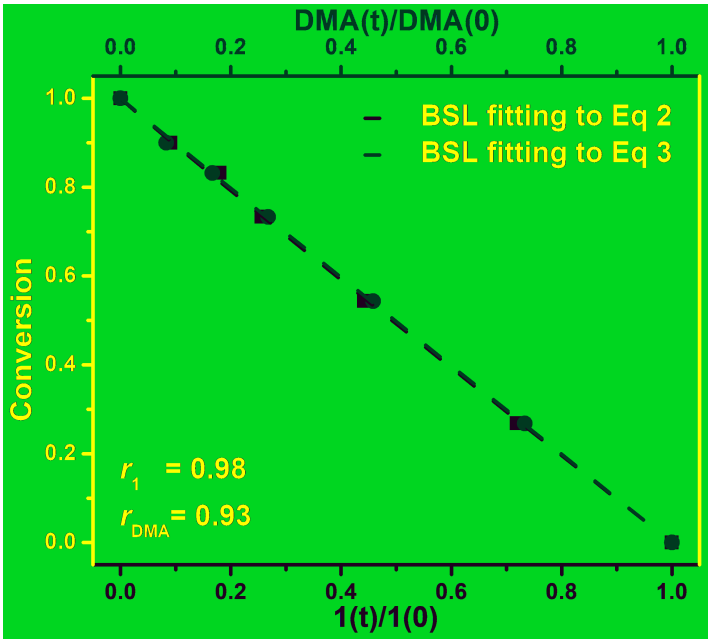

Figure S10. The plot of total conversion with respect to [**1**(t)]/[**1**(0)] and [DMA(t)]/[DMA(0)] is fitted to Eq. 2 and Eq. 3 of the BSL integrated model independently to derive the comonomer reactivity ratios for the copolymerization of **1** and DMA at $f_1^0 = 0.09$.

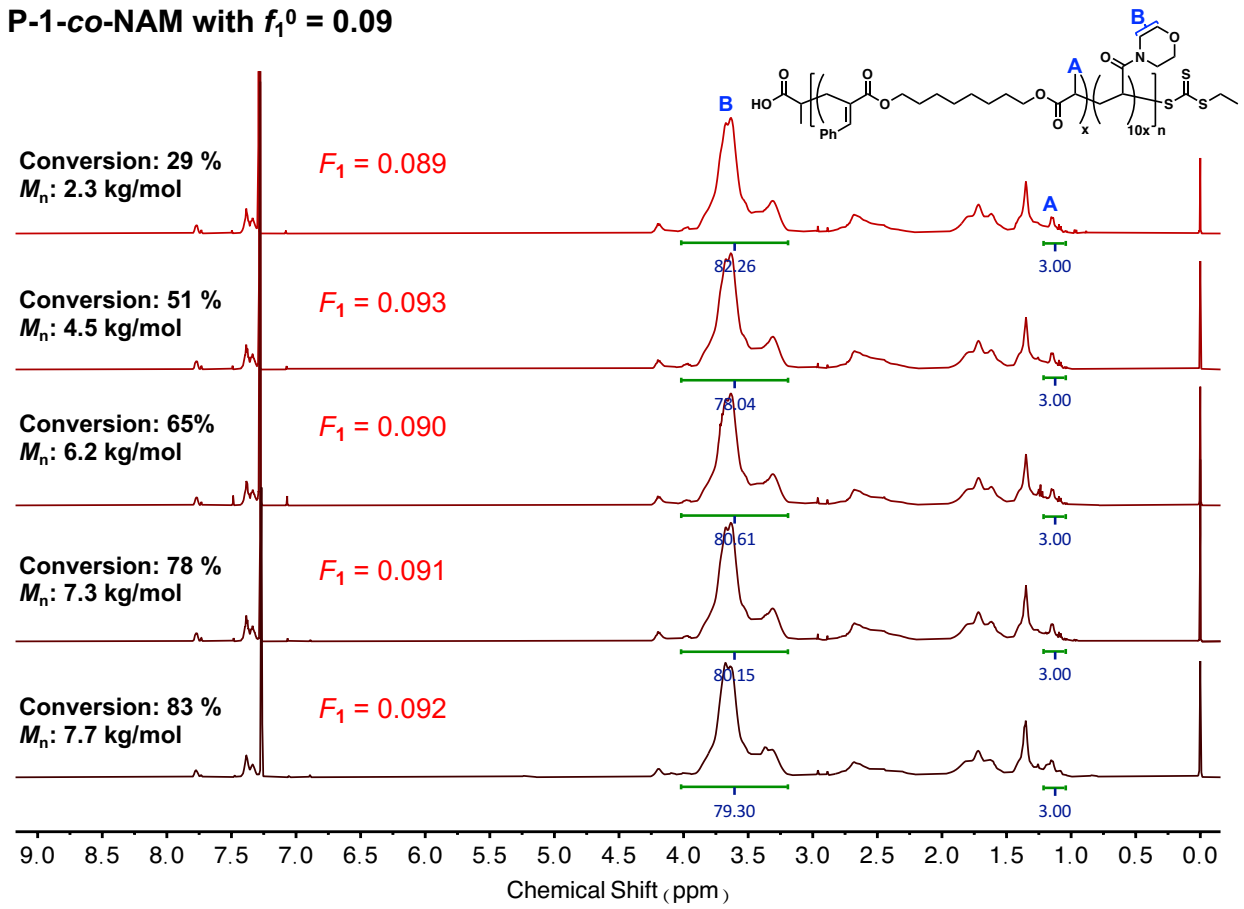

Figure S11. Compositional analysis of **P-1-*co*-NAM** at f_1^0 = 0.09 at different time points of the copolymerization by ^{1}H NMR. The incorporation of **1** in **P-1-*co*-NAM** (F_1) was determined by the following equation:

$$F_1 = \frac{8 \times I_A}{8 \times I_A + 3 \times I_B}$$

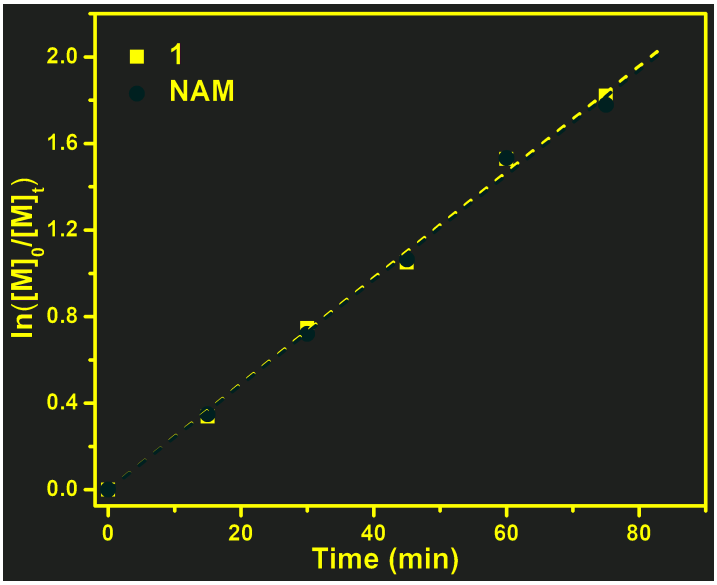

Figure S12. Kinetic plots of the organocatalyzed photocontrolled radical ring-opening cascade copolymerization of **1** and NAM at $f_1^0 = 0.09$.

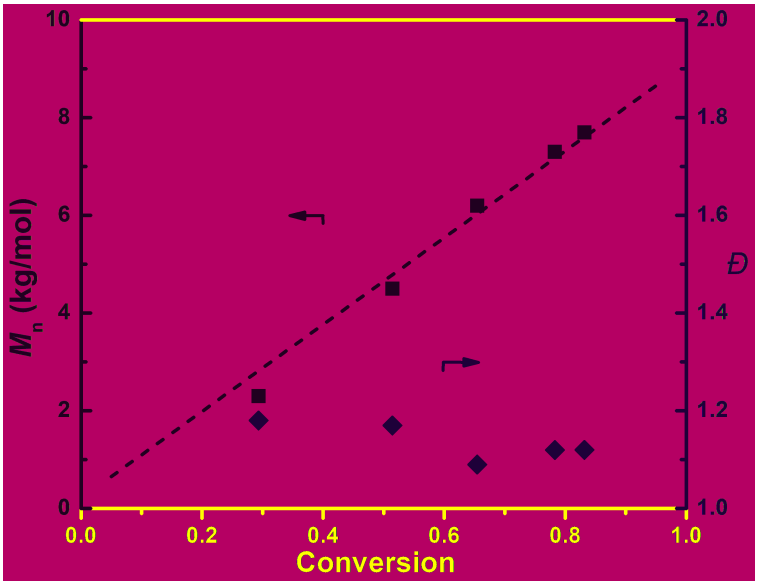

Figure S13. Plots of M_n and $Đ$ of **P-1-*co*-NAM** as a function of total conversion.

Table S5. The summary of copolymerization results of **1** and NAM at $f_1^0 = 0.09$ at different time points.

Time (min)	**1**(t)/**1**(0)	NAM(t)/NAM(0)	*conv.*
15	0.71	0.71	0.29
30	0.47	0.49	0.51
45	0.35	0.35	0.65
60	0.22	0.22	0.78
75	0.16	0.17	0.83

The reactivity ratios of **1** and NAM were derived through a nonlinear fitting of the respective instantaneous concentrations of **1** and NAM at various *conv.* values to Eq. 2 and Eq. 3 independently.

$$conv. = 1 - f_1^0 \left[\frac{\mathbf{1}(t)}{\mathbf{1}(0)}\right] - (1 - f_1^0) \left[\frac{\mathbf{1}(t)}{\mathbf{1}(0)}\right]^{r_{\mathrm{NAM}}} \quad (2)$$

$$conv. = 1 - f_1^0 \left[\frac{\mathrm{NAM}(t)}{\mathrm{NAM}(0)}\right]^{r_1} - (1 - f_1^0) \left[\frac{\mathrm{NAM}(t)}{\mathrm{NAM}(0)}\right] \quad (3)$$

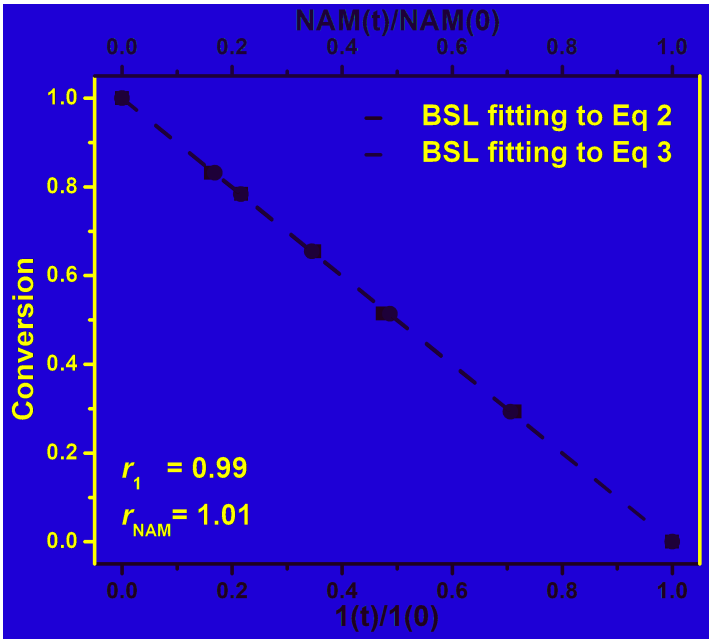

Figure S14. The plot of total conversion with respect to [**1**(t)]/[**1**(0)] and [NAM(t)]/[NAM(0)] is fitted to Eq. 2 and Eq. 3 of the BSL integrated model independently to derive the comonomer reactivity ratios for the copolymerization of **1** and NAM at $f_1^0 = 0.09$.

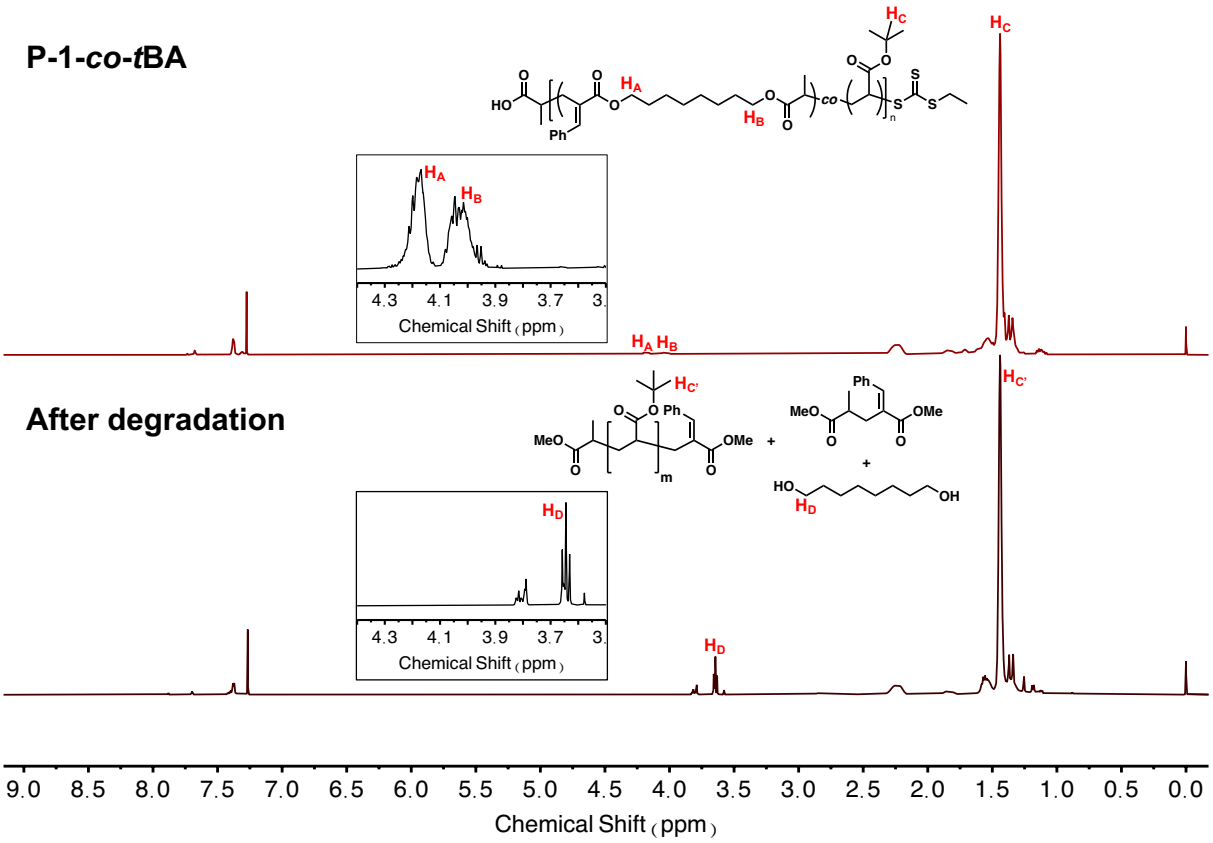

Figure S15. The ^{1}H NMR analysis of the degradation of **P-1-*co*-*t*BA**.

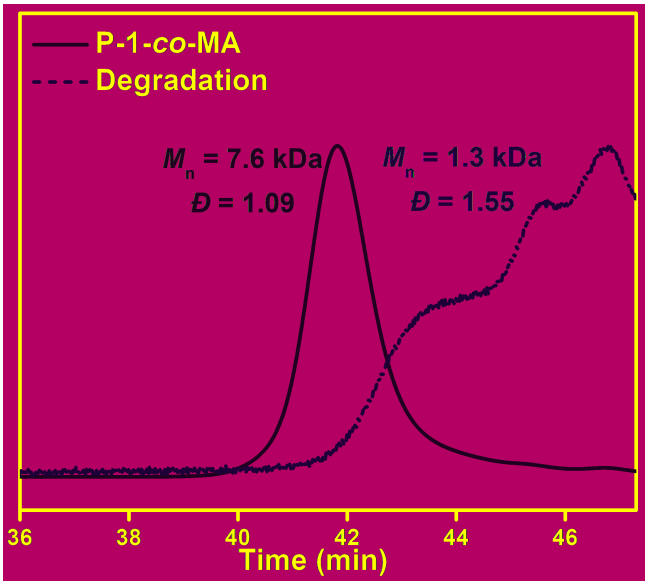

Figure S16. The degradation of **P-1-*co*-MA** exhibited a clear shift to the lower molecular region on SEC.

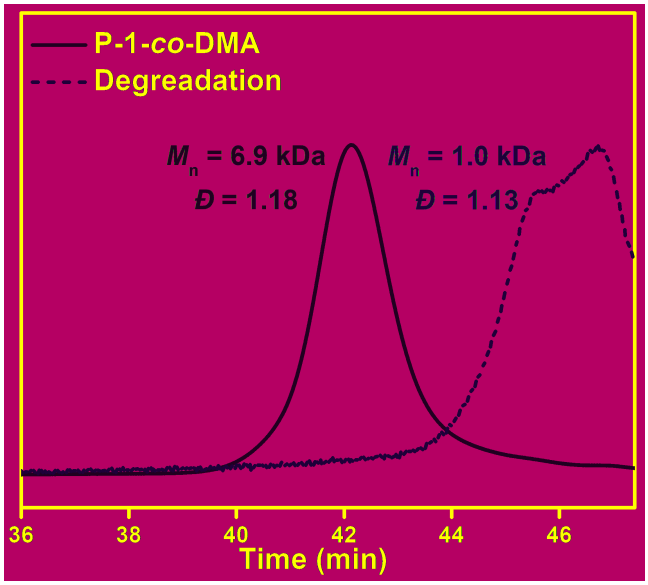

Figure S17. The degradation of **P-1-*co*-DMA** exhibited a clear shift to the lower molecular region on SEC.

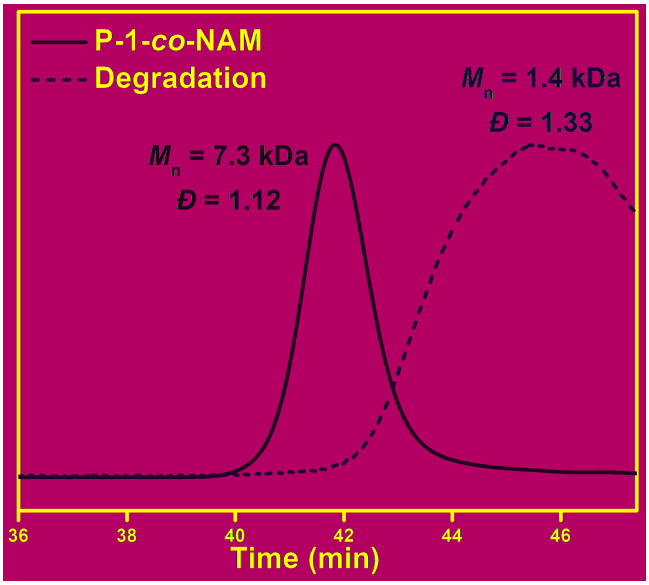

Figure S18. The degradation of **P-1-*co*-NAM** exhibited a clear shift to the lower molecular region on SEC.

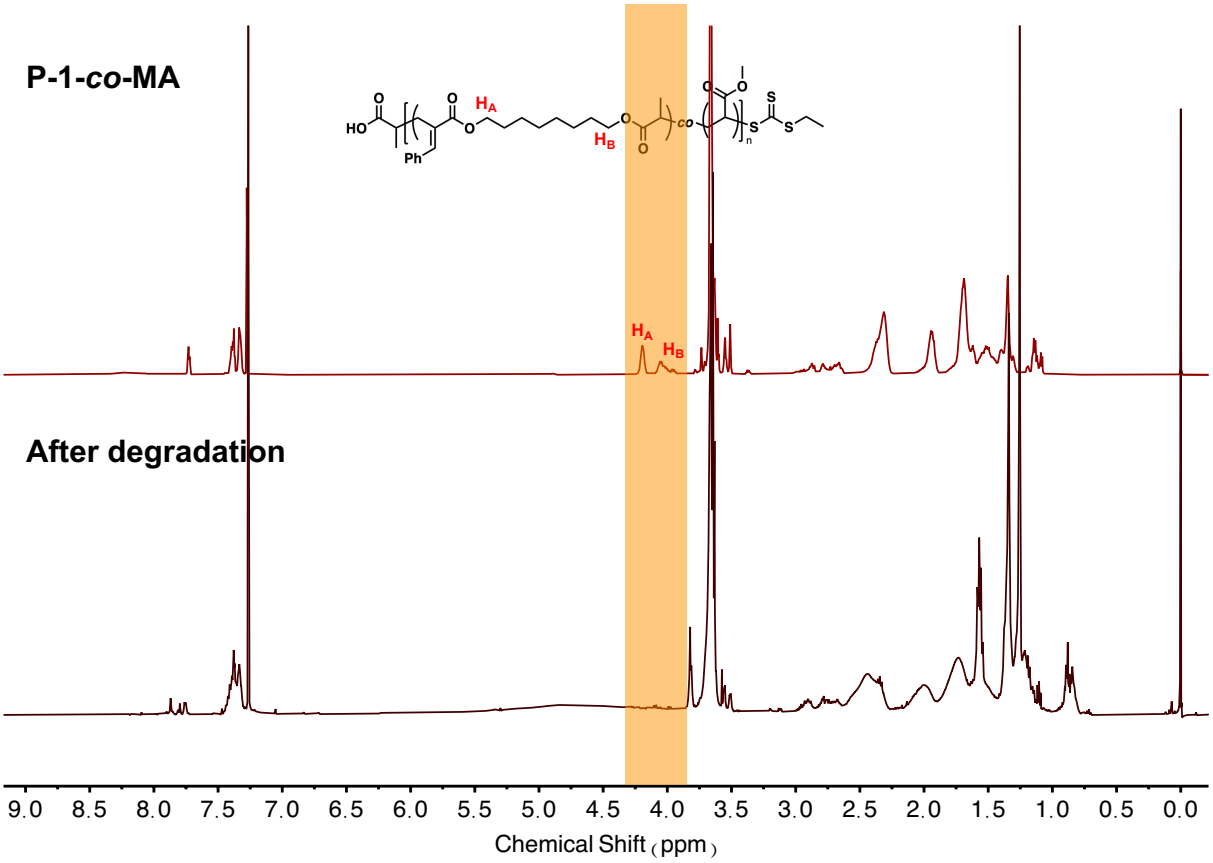

Figure S19. The ^{1}H NMR analysis of the degradation of **P-1-*co*-MA**.

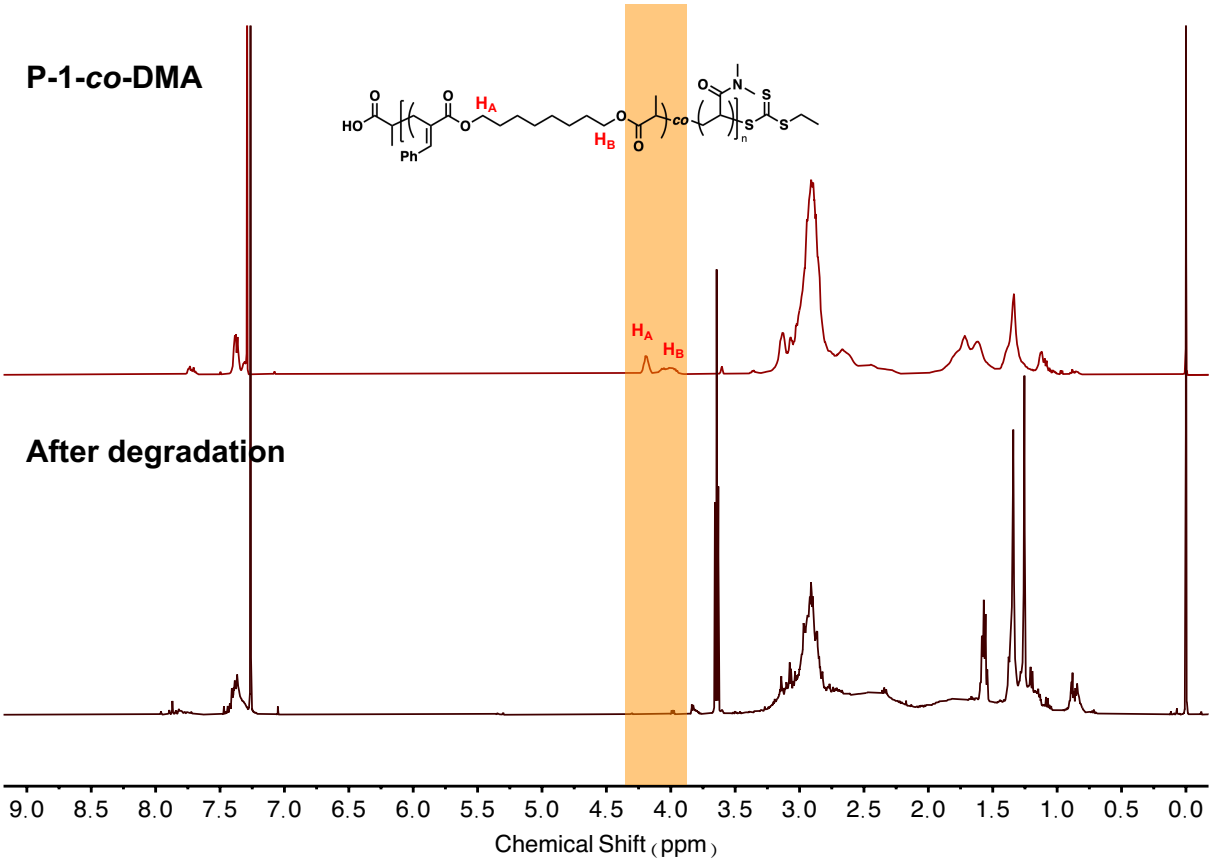

Figure S20. The ^{1}H NMR analysis of the degradation of **P-1-*co*-DMA**.

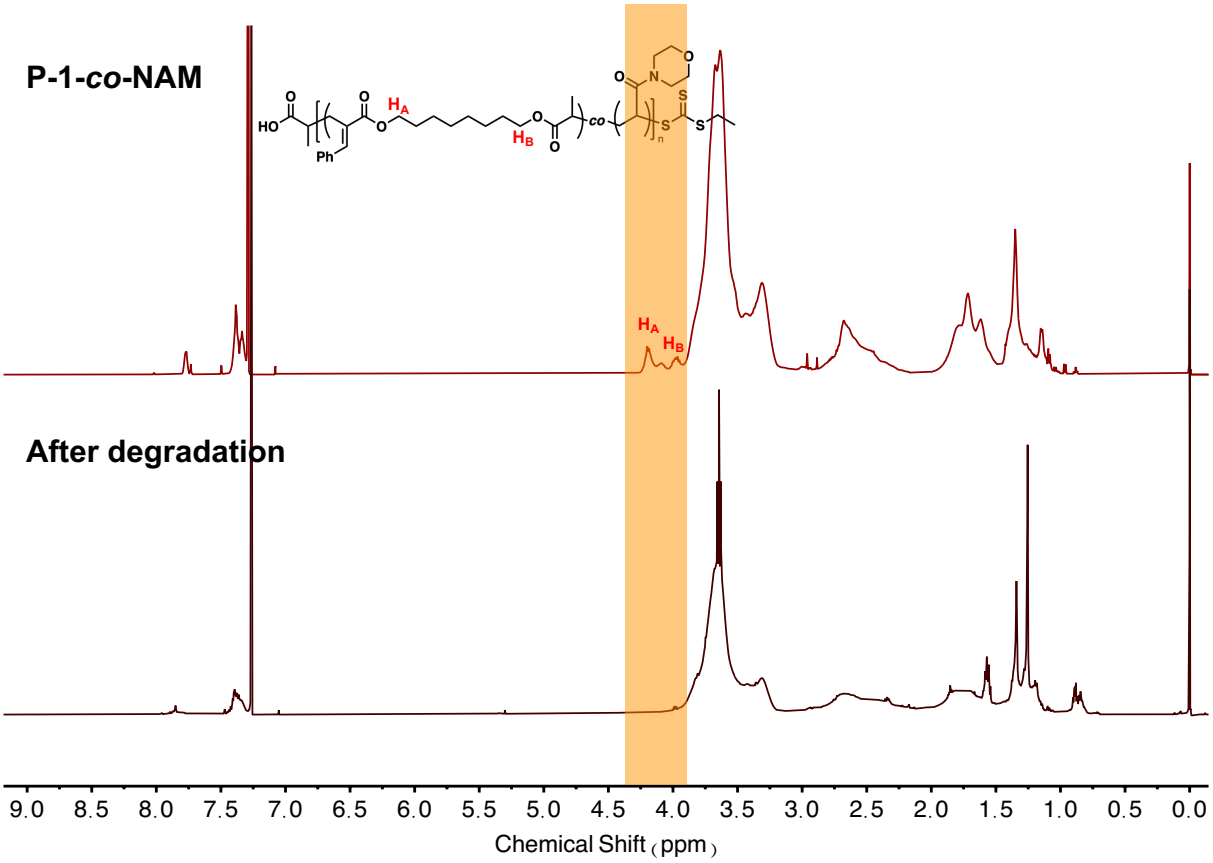

Figure S21. The ^{1}H NMR analysis of the degradation of **P-1-*co*-NAM**.

Table S6. The summary of copolymerization results of **1** and St at f_1^0 = 0.09 at different time points.

Time (h)	**1**(t)/**1**(0)	St(t)/St(0)	*conv.*
12	0.70	0.91	0.11
20	0.51	0.81	0.22
30	0.41	0.75	0.28
40	0.29	0.63	0.40
50	0.24	0.59	0.44

The reactivity ratios of **1** and St were derived through a nonlinear fitting of the respective instantaneous concentrations of **1** and St at various *conv.* values to Eq. 2 and Eq. 3 independently.

$$conv. = 1 - f_{\mathbf{1}}^0 \left[\frac{\mathbf{1}(t)}{\mathbf{1}(0)}\right] - (1 - f_{\mathbf{1}}^0) \left[\frac{\mathbf{1}(t)}{\mathbf{1}(0)}\right]^{r_{\mathrm{St}}} \quad (2)$$

$$conv. = 1 - f_{\mathbf{1}}^0 \left[\frac{\mathrm{St}(t)}{\mathrm{St}(0)}\right]^{r_{\mathbf{1}}} - (1 - f_{\mathbf{1}}^0) \left[\frac{\mathrm{St}(t)}{\mathrm{St}(0)}\right] \quad (3)$$

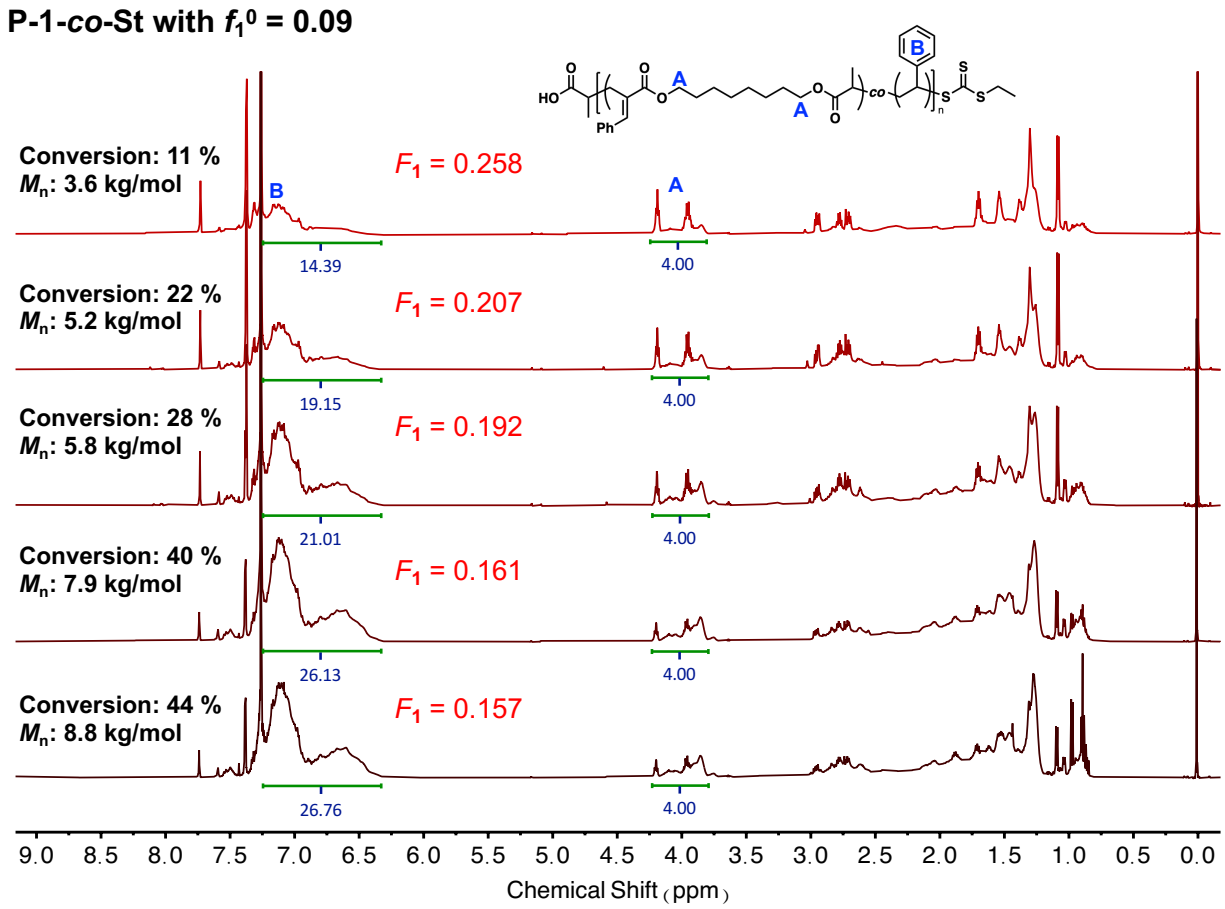

Figure S22. Compositional analysis of **P-1-*co*-St** at f_1^0 = 0.09 at different time points of the copolymerization by ^{1}H NMR. The incorporation of **1** in **P-1-*co*-St** (F_1) was determined by the following equation:

$$F_1 = \frac{5 \times I_A}{5 \times I_A + 4 \times I_B}$$

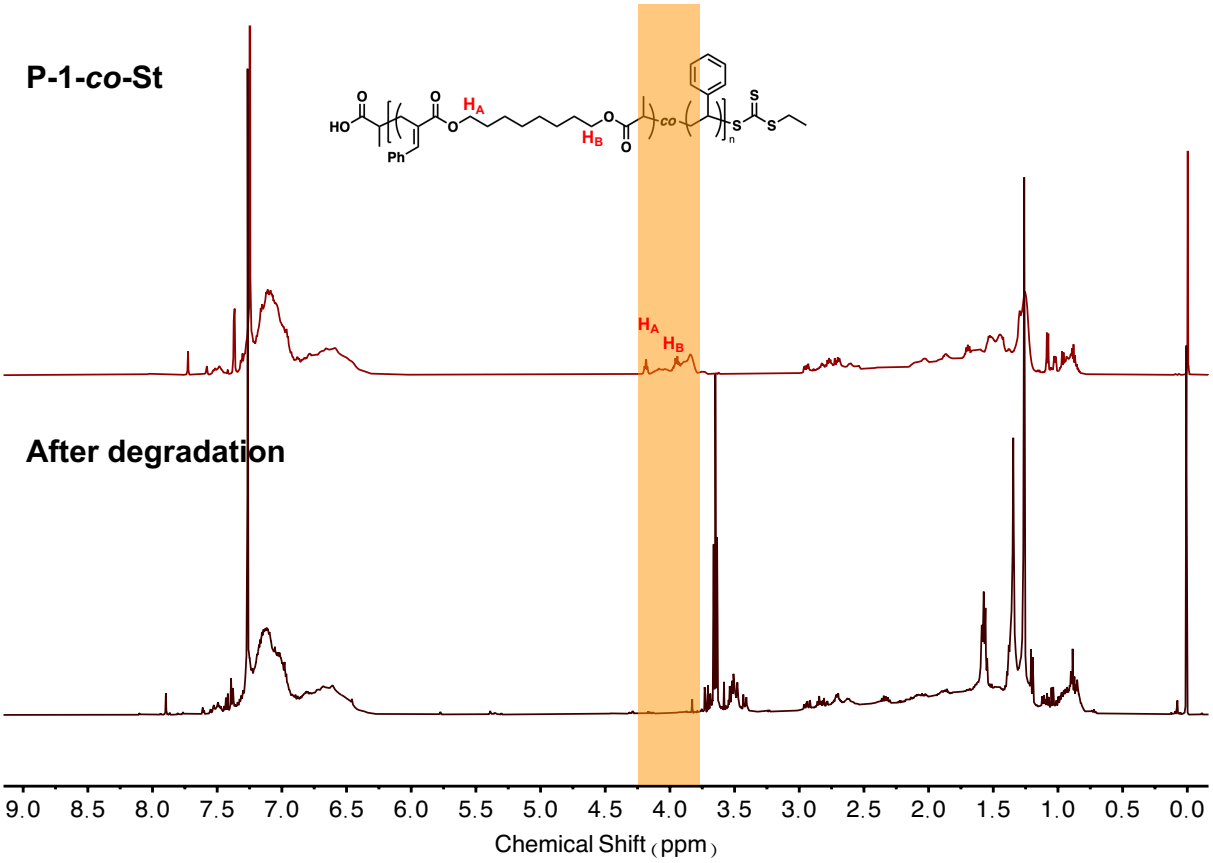

Figure S23. The ^{1}H NMR analysis of the degradation of **P-1-*co*-St**.

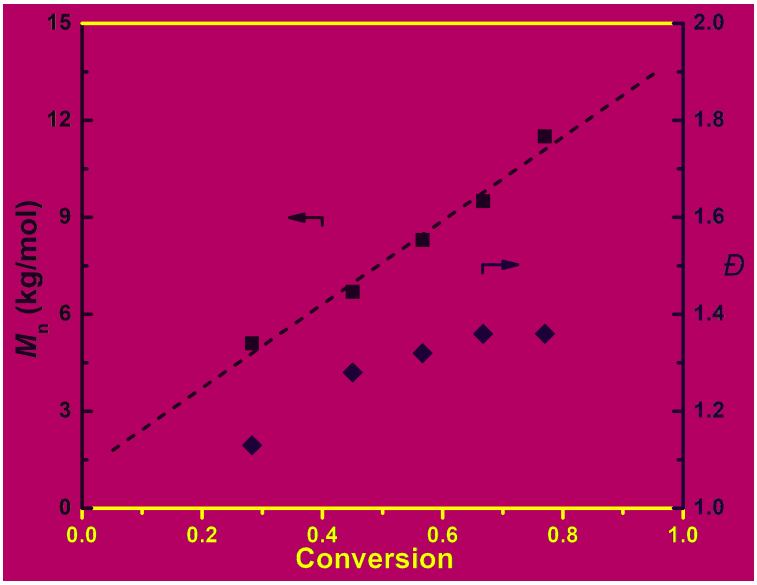

Figure S24. Plots of M_n and $Đ$ of **P-1-*co*-MMA** as a function of total conversion.

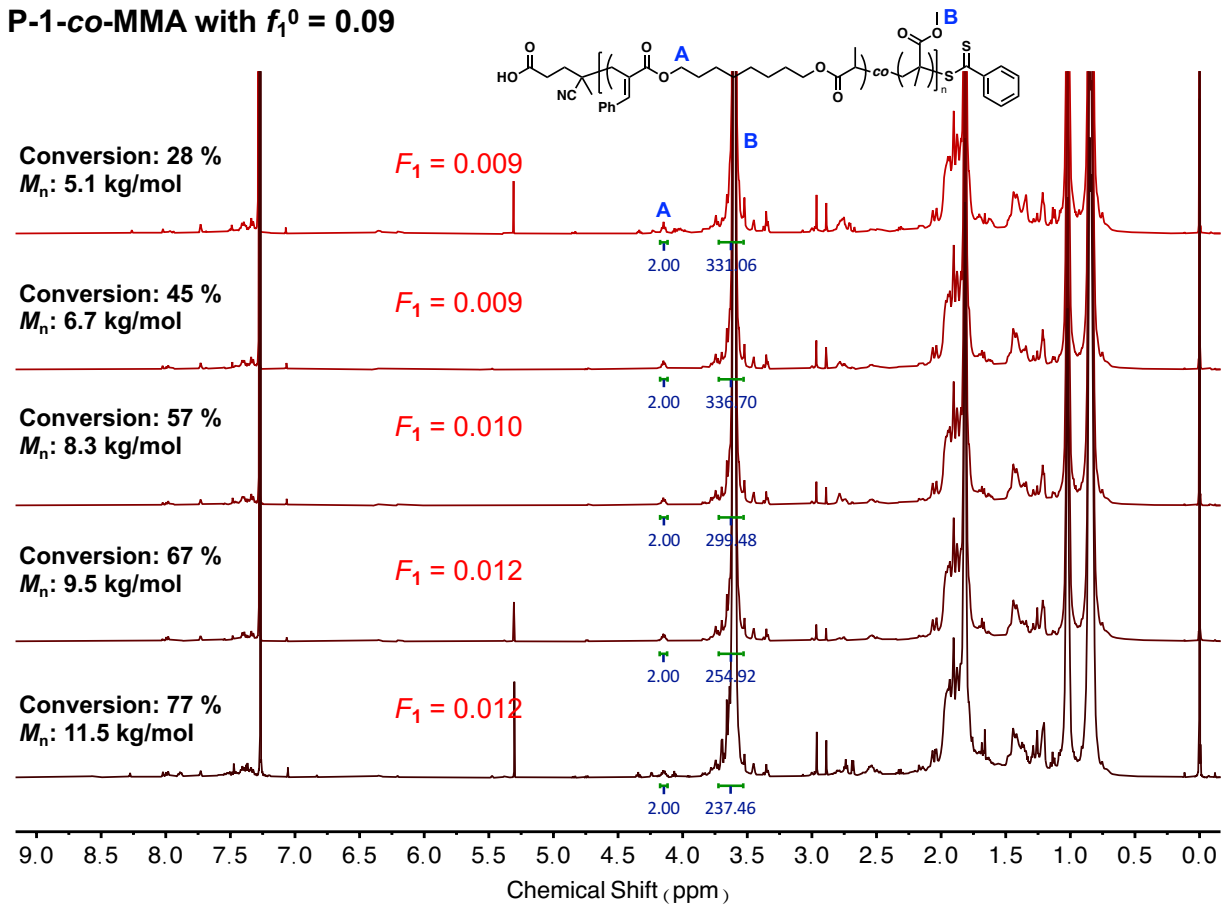

Figure S25. Compositional analysis of **P-1-*co*-MMA** at f_1^0 = 0.09 at different time points of the copolymerization by ^{1}H NMR. The incorporation of **1** in **P-1-*co*-MMA** (F_1) was determined by the following equation:

$$F_1 = \frac{3 \times I_A}{3 \times I_A + 2 \times I_B}$$

Table S7. The summary of copolymerization results of **1** and MMA at $f_1^0 = 0.09$ at different time points.

Time (h)	**1**(t)/**1**(0)	MMA(t)/MMA(0)	*conv.*
10	0.95	0.70	0.28
20	0.90	0.52	0.45
30	0.85	0.39	0.57
40	0.79	0.29	0.67
50	0.74	0.18	0.77

The reactivity ratios of **1** and MMA were derived through a nonlinear fitting of the respective instantaneous concentrations of **1** and MMA at various *conv.* values to Eq. 2 and Eq. 3 independently.

$$conv. = 1 - f_{\mathbf{1}}^0 \left[\frac{\mathbf{1}(t)}{\mathbf{1}(0)}\right] - (1 - f_{\mathbf{1}}^0) \left[\frac{\mathbf{1}(t)}{\mathbf{1}(0)}\right]^{r_{\mathrm{MMA}}} \quad (2)$$

$$conv. = 1 - f_{\mathbf{1}}^0 \left[\frac{\mathrm{MMA}(t)}{\mathrm{MMA}(0)}\right]^{r_{\mathbf{1}}} - (1 - f_{\mathbf{1}}^0) \left[\frac{\mathrm{MMA}(t)}{\mathrm{MMA}(0)}\right] \quad (3)$$

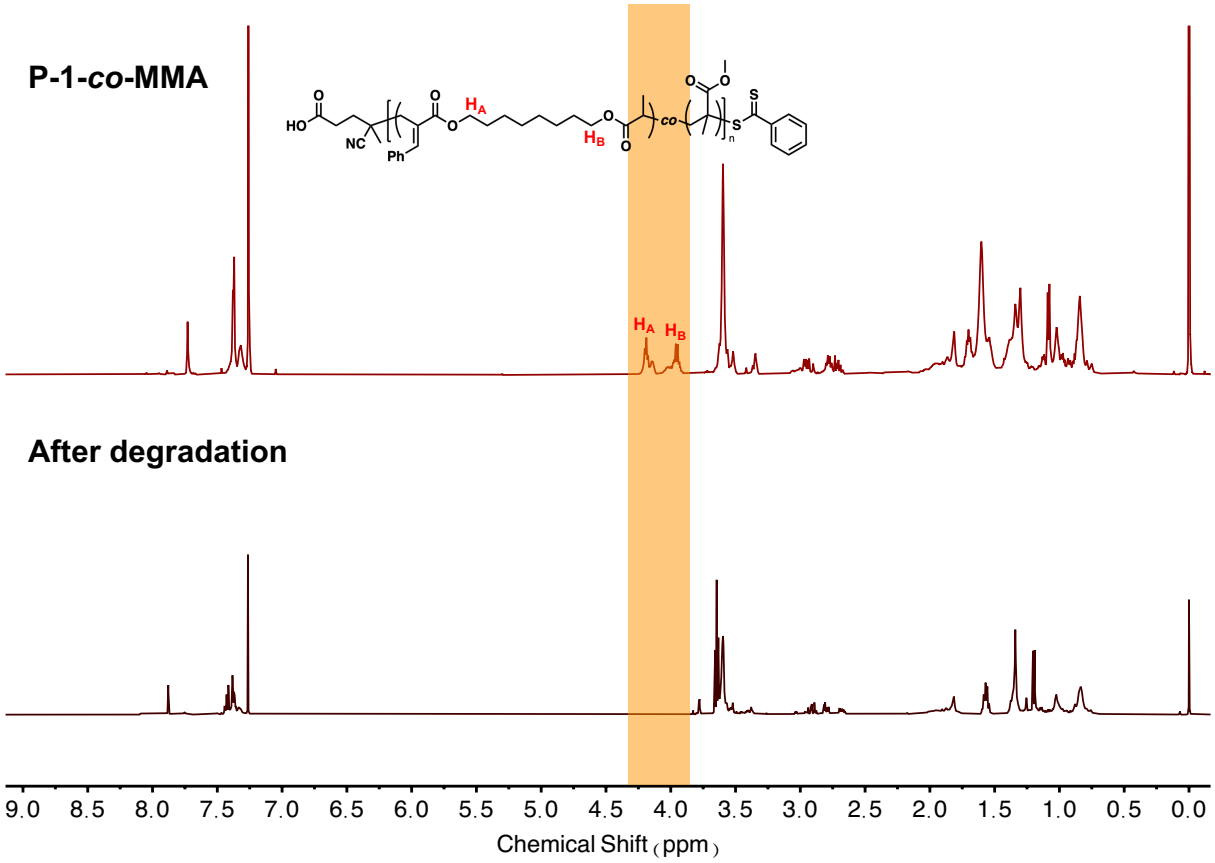

Figure S26. The ^{1}H NMR analysis of the degradation of **P-1-*co*-MMA**.

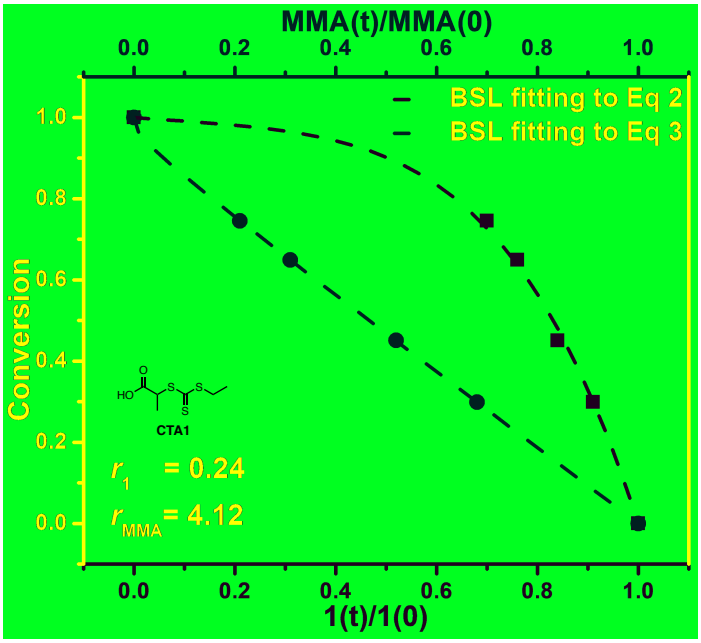

Figure S27. The plot of total conversion with respect to [**1**(t)]/[**1**(0)] and [MMA(t)]/[MMA(0)] is fitted to Eq. 2 and Eq. 3 of the BSL integrated model independently to derive the comonomer reactivity ratios for the copolymerization of **1** and MMA at $f_1^0 = 0.09$ when **CTA1** is used as chain transfer agent.

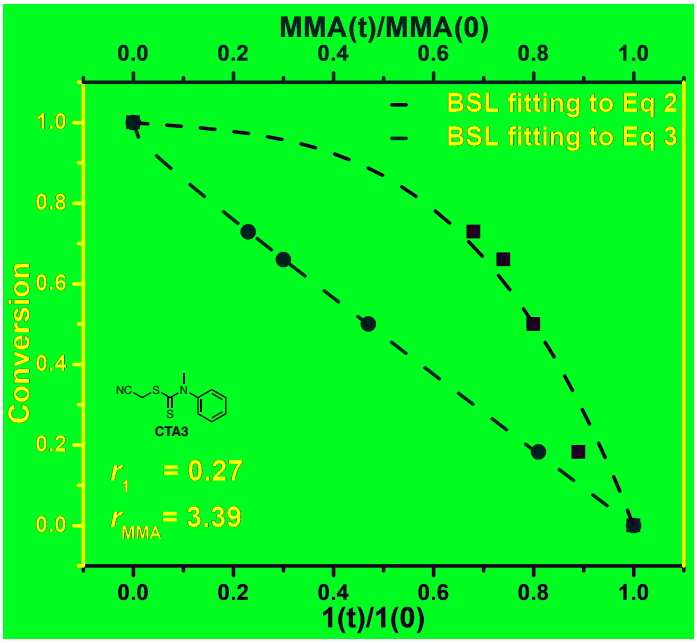

Figure S28. The plot of total conversion with respect to [**1**(t)]/[**1**(0)] and [MMA(t)]/[MMA(0)] is fitted to Eq. 2 and Eq. 3 of the BSL integrated model independently to derive the comonomer reactivity ratios for the copolymerization of **1** and MMA at $f_1^0 = 0.09$ when **CTA3** is used as chain transfer agent.

Table S8. The summary of degradation of **P-1-*co*-St** at different conversions.

conv.	F_1	M_n	Degraded M_n
11 %	0.26	3.6 kg mol^{-1}	1.0 kg mol^{-1}
22 %	0.21	5.2 kg mol^{-1}	1.1 kg mol^{-1}
28 %	0.19	5.8 kg mol^{-1}	1.2 kg mol^{-1}
40 %	0.16	7.9 kg mol^{-1}	1.3 kg mol^{-1}
44 %	0.15	8.8 kg mol^{-1}	1.4 kg mol^{-1}

Supplementary Methods

Materials. Organic solvents, including dimethylformamide (DMF), were bought from Fisher Scientific and purified by solvent purification systems (Pure Process Technology). Chain transfer agents were synthesized according to the reported procedures.[1] Chemicals were bought from Sigma-Aldrich, Strem Chemical, or Fisher Scientific and used without further purification.

Instrumentation and Characterization. Photocontrolled polymerizations were performed in a HepatoChem EvoluChem PhotoRedOx Box TC with an EvoluChem LED spotlight (P201-18-2, 450 nm, 18W) equipped with a recirculating chiller. Silica gel column chromatography was carried out using an automated flash chromatography (Biotage). ^{1}H NMR spectra were recorded in $CDCl_3$ by a Varian 600 MHz spectrometer, a Varian 500 MHz spectrometer, and two Bruker AVANCE NEO 500 MHz spectrometers, one with a Prodigy and the other with a Helium CryoProbe, using residual chloroform (δ = 7.26 for ^{1}H) as internal standard. The mass spectrum was obtained using a Bruker Auto Flex Max instrument (positive mode). α-Cyano-4-hydroxycinnamic acid was used as the matrix with NaI added as the cation source for the polymer. Size-exclusion chromatography (SEC) measurements were performed on a Tosoh's high-performance SEC system HLC-8320GPC with TSKgel Alpha-M columns at 50 ºC and a flow rate of 0.6 mL/min. HPLC grade DMF with 0.01 M LiBr was used as the eluent. Polystyrene standards (ReadyCal Kit, Sigma-Aldrich #81434) were used to determine the molecular weight and molecular weight distribution of polymers. The polymers were dissolved in the above DMF solution and filtered through a 0.20 μm PTFE filter before being injected into the SEC system. Differential scanning calorimetry (DSC) and thermogravimetric analysis (TGA) measurements were performed on a Netzsch Instruments STA 449 F1 Jupiter at a ramp of 10 ºC/min.

Scheme S1. General procedure of the organocatalyzed photocontrolled radical homopolymerization of macrocyclic allylic sulfone.

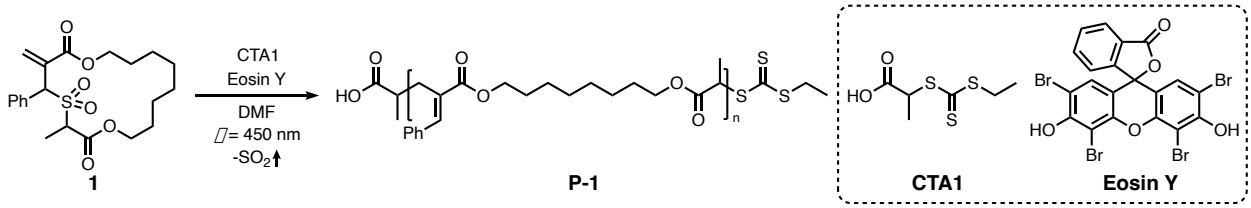

The organocatalyzed photocontrolled radical homopolymerization of macrocyclic allylic sulfone **1** was performed under nitrogen in 4 mL glass vials equipped with TFE lined silicone SURE-LINK septa (Chemglass CG-4909-04) using a HepatoChem EvoluChem PhotoRedOx Box TC with an EvoluChem LED spotlight (P201-18-2, 450 nm, 18W) equipped with a recirculating chiller. The macrocyclic allylic sulfone **1** was prepared following the reported procedures.[2] The stock solution of **1**, **CTA1**, and eosin Y was prepared and stored in the fridge (4 ºC). In a 4 mL glass vial equipped with a stir bar was charged with allylic sulfone macrocyclic monomer (0.1 mmol), CTA (2.00 μmol), eosin Y (0.1 μmol), and DMF (0.2 mL). The mixture was covered under aluminum foil and degassed by nitrogen for 20 minutes. The mixture was then irradiated by a blue LED spotlight (18 W, λ_{max} = 450 nm) at room temperature. The vial was exposed to air to stop the polymerization. The reaction mixture was diluted with dichloromethane (DCM) and precipitated in hexane for three times. The resulting polymers were analyzed by ^{1}H NMR and SEC. ^{1}H NMR data matches that in the literature.[2]

Scheme S2. Procedure for the synthesis of diblock copolymers **P-1-*b*-PMA**.

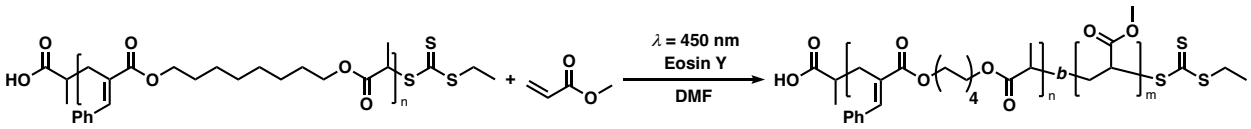

In a 4 mL glass vial equipped with a stir bar was charged with allylic sulfone macrocyclic monomer **1** (0.2 mmol), **CTA1** (5 μmol), eosin Y (0.2 μmol), and DMF (0.4 mL). The mixture was covered under aluminum foil and degassed by nitrogen for 20 minutes. The mixture was then irradiated by a blue LED spotlight (18 W, λ_{max} = 450 nm) at room temperature for 4 hours. The monomer conversion was monitored by ^{1}H NMR (64% conversion of **1**). The vial was then exposed to air to stop the polymerization. The reaction mixture was diluted with DCM and precipitated in hexane for three times. The resulting polymers were analyzed by ^{1}H NMR and SEC.

In a 4 mL glass vial equipped with a stir bar was charged with methyl acrylate (MA) (0.4 mmol), macroinitiator **P-1** (2 μmol), eosin Y (0.4 μmol), and DMF (0.8 mL). The mixture was covered by aluminum foil and degassed by nitrogen at 0 ºC for 20 minutes. The mixture was then irradiated by a blue LED spotlight (18 W, λ_{max} = 450 nm) at room temperature for 4 hours. The monomer conversion was monitored by ^{1}H NMR (69% conversion of MA). The vial was then exposed to air to stop the polymerization. The reaction mixture was diluted with DCM and precipitated in hexane for three times. The resulting polymers were analyzed by ^{1}H NMR and SEC.

Scheme S3. General procedure for the synthesis and degradation of degradable vinyl copolymers from the organocatalyzed photocontrolled radical ring-opening cascade copolymerization.

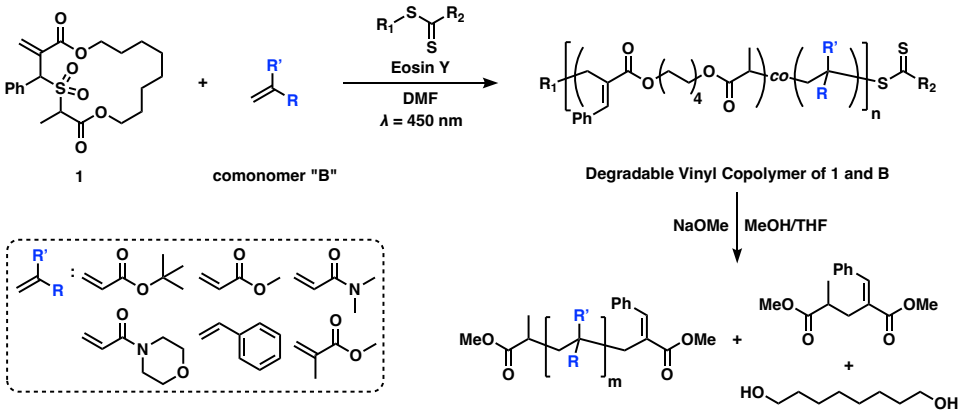

Copolymerization of macrocyclic allylic sulfone and vinyl monomers. In a 4 mL glass vial equipped with a stir bar was charged with allylic sulfone macrocyclic monomer (0.1 mmol), vinyl comonomer (1 mmol), CTA (10.0 μmol), EY (1.1 μmol), and DMF (0.2 mL). The mixture was covered under aluminum foil and degassed by nitrogen at 0 ºC for 20 min. The mixture was then irradiated by a blue LED spotlight (18 W, λ_{max} = 450 nm) at room temperature. The vial was exposed to air to stop the polymerization. The reaction mixture was diluted with DCM and precipitated in hexane for three times. The resulting polymers were analyzed by ^{1}H NMR and SEC.

Degradation of degradable vinyl copolymers. In a 4 mL glass vial equipped with a stir bar, 10 mg degradable vinyl copolymers were dissolved in 0.5 mL THF. A solution of sodium methoxide (100 μL of a 25 wt% solution in methanol) was added. After 30 min, the reaction was stopped by the addition of a 1 M aqueous hydrochloric acid. To collect the degraded products for ^{1}H NMR and SEC analyses, the mixture was extracted with DCM. The organic phase was dried with Na_2SO_4 and concentrated *in vacuo*.

Determination of monomer conversion by ^{1}H NMR. The monomer conversion for the polymerization of macrocyclic allylic sulfone **1** was determined based on the assignment that the integral of the doublet at δ = 1.09 ppm (Peak *a*, Figure S29) corresponds to the methyl group of the polymer **P-1** (3H), and the integral of the singlet at δ = 6.76 ppm (Peak *b*, Figure S29) corresponds to terminal alkene of unreacted monomer (1H). When the integral of Peak *a* is normalized, the monomer conversion θ is calculated based on the following equation, where I_b is the integral of peak *b*.

$$\theta = \frac{1}{1 + 3 \times I_b} \times 100\%$$

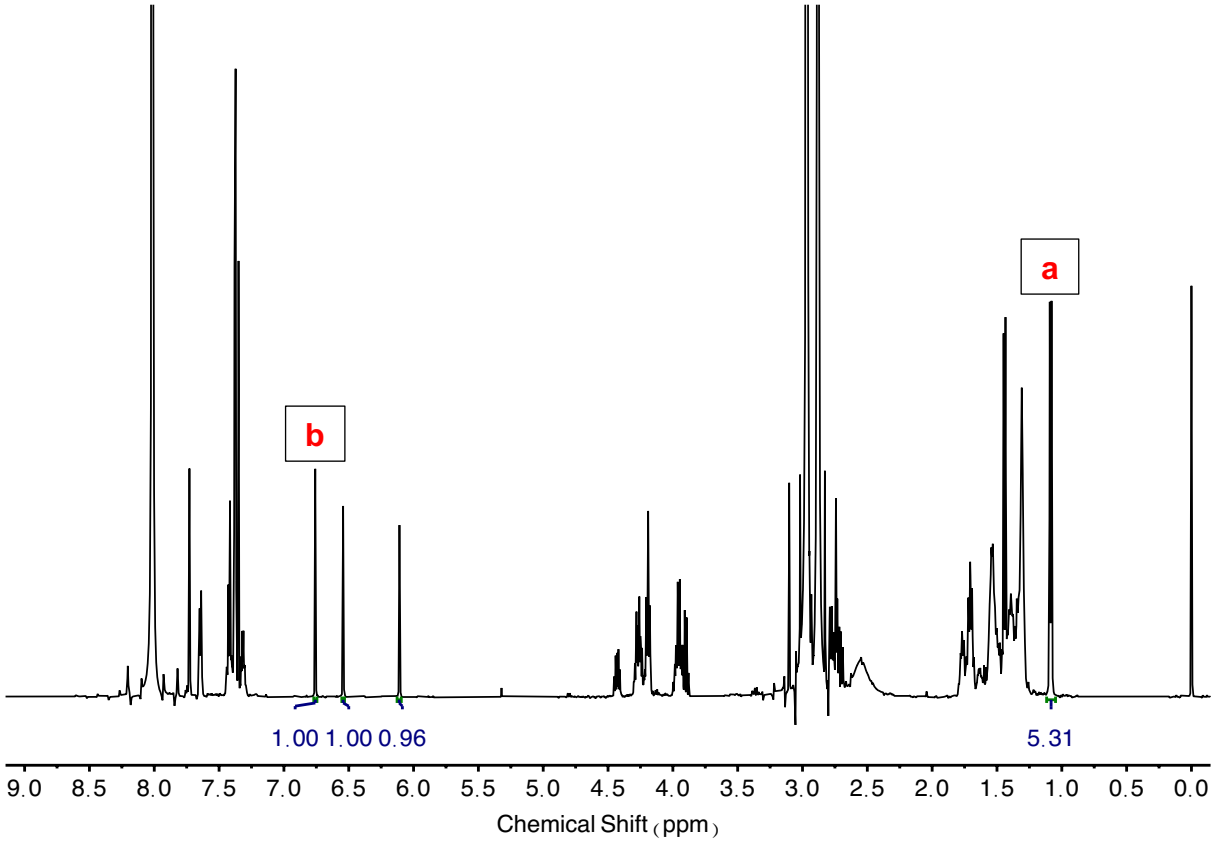

Figure S29. ^{1}H NMR determination of monomer conversion for the organocatalyzed photoredox radical homopolymerization of macrocyclic allylic sulfone **1**.

Determination of comonomer conversions for the copolymerization of 1 and MA. The comonomer conversions for the copolymerization of **1** and MA were determined based on the assignments that the integral of the multiplet at δ = 1.13 ppm (Peak *a*, Figure S30) corresponds to the methyl group of **P-1** unit (3H); the integral of the singlet at δ = 6.55 ppm (Peak *b*, Figure S30) corresponds to the terminal alkene of unreacted allylic sulfone macrocyclic monomer **1** (1H); the integral of the singlet at δ = 3.75 ppm (Peak *c*, Figure S30) corresponds to the methyl group of unreacted MA (3H); and the integral of the singlet at δ = 3.67 ppm (Peak *d*, Figure S30) corresponds to the methyl group of PMA unit (3H). The monomer conversion θ of **1** and MA is calculated based on the following equation, where I_a is the integral of peak *a*, I_b is the integral of peak *b*, I_c is the integral of peak *c*, and I_d is the integral of peak *d*.

$$\theta_{\mathbf{1}} = \frac{I_a}{I_a + 3 \times I_b} \times 100\% \qquad \theta_{\mathbf{MA}} = \frac{I_d}{I_c + I_d} \times 100\%$$

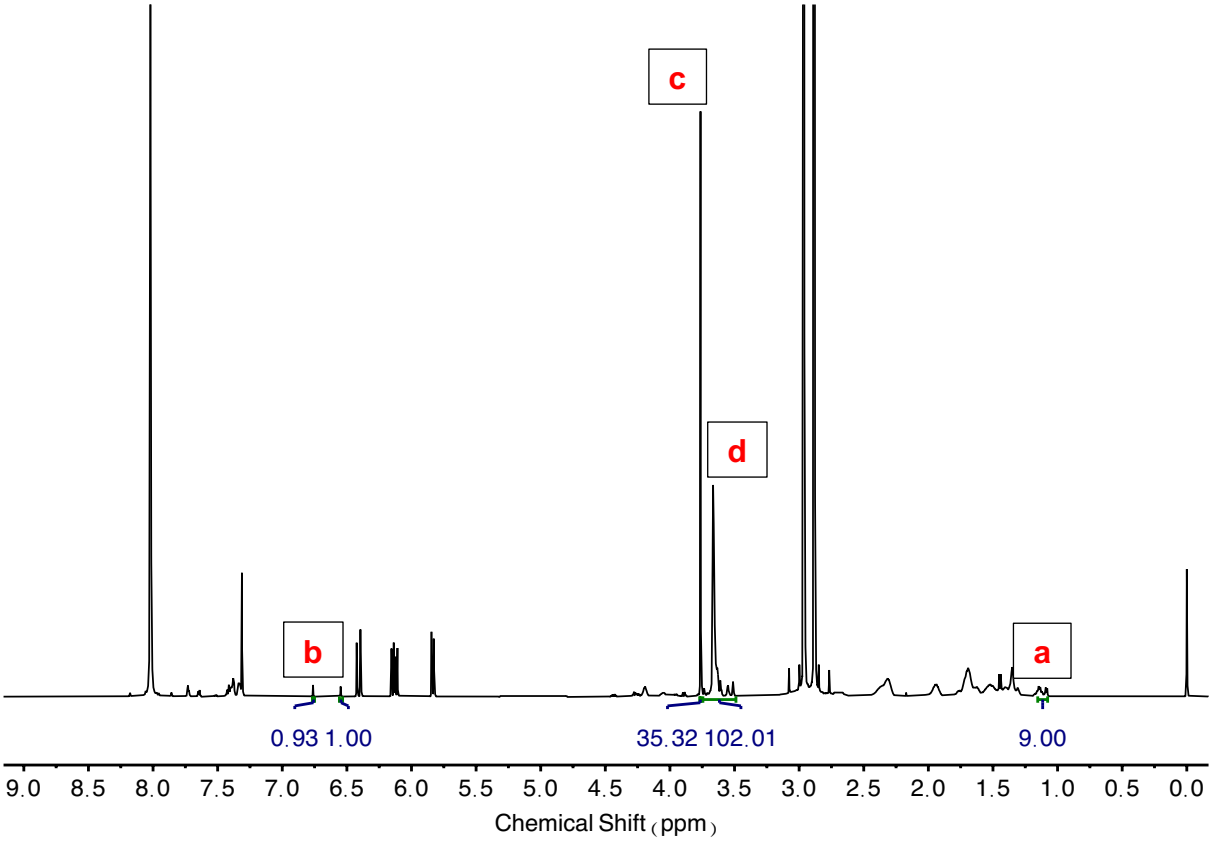

Figure S30. ^{1}H NMR analysis of the photocontrolled organocatalyzed radical ring-opening cascade copolymerization of allylic sulfone macrocyclic monomer **1** and MA.

References.

1. Skey, J.; O'Reilly, R. K. Facile one pot synthesis of a range of reversible addition-fragmentation chain transfer (RAFT) agents. *Chem. Commun*. **2008**, *44*, 4183-4185.
2. Wang, W.; Zhou, Z.; Sathe, D.; Tang, X.; Moran, S.; Jin, J.; Haeffner, F.; Wang, J.; Niu, J. Degradable Vinyl Random Copolymers via Photocontrolled Radical Ring-Opening Cascade Copolymerization. *Angew. Chem., Int. Ed.* **2021**, *61*, e202113302.

^{1}H NMR of block copolymer **P-1-*b*-PMA**.

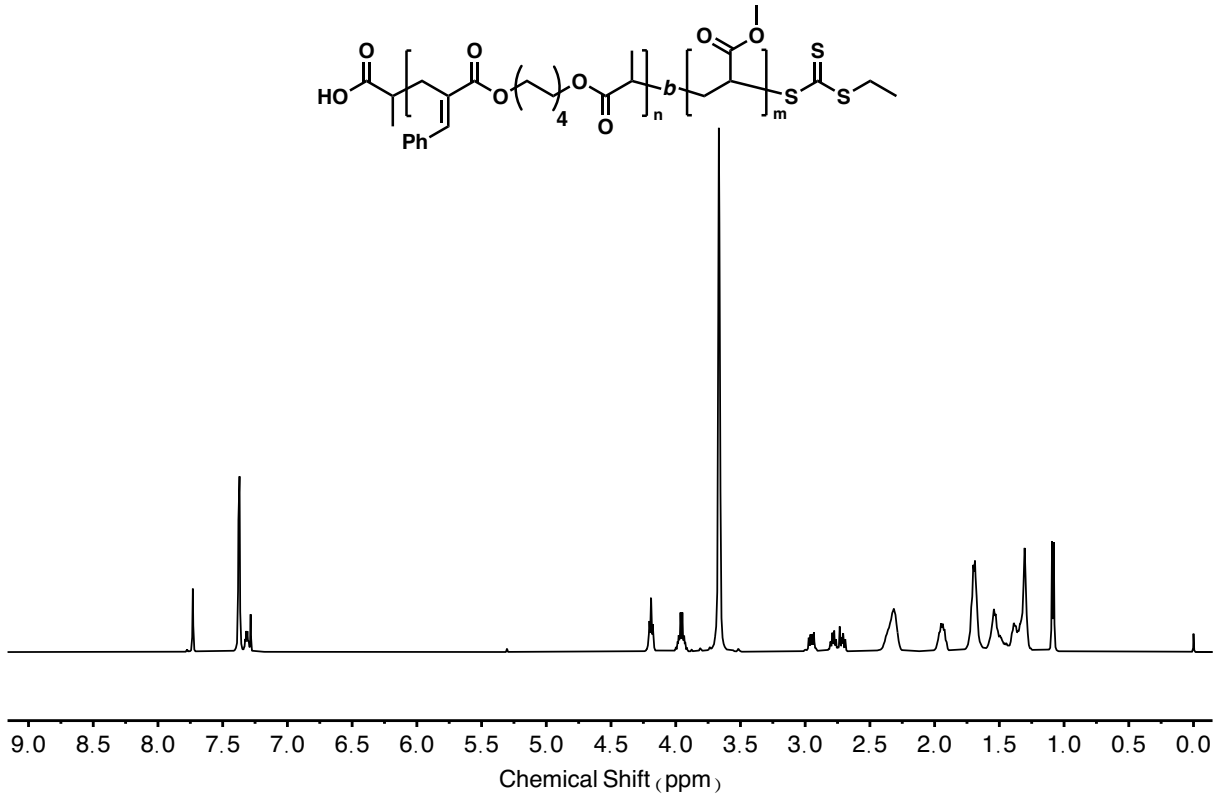

^{1}H NMR of degradable vinyl copolymer **P-1-*co*-St** at f_1^0 = 0.09.

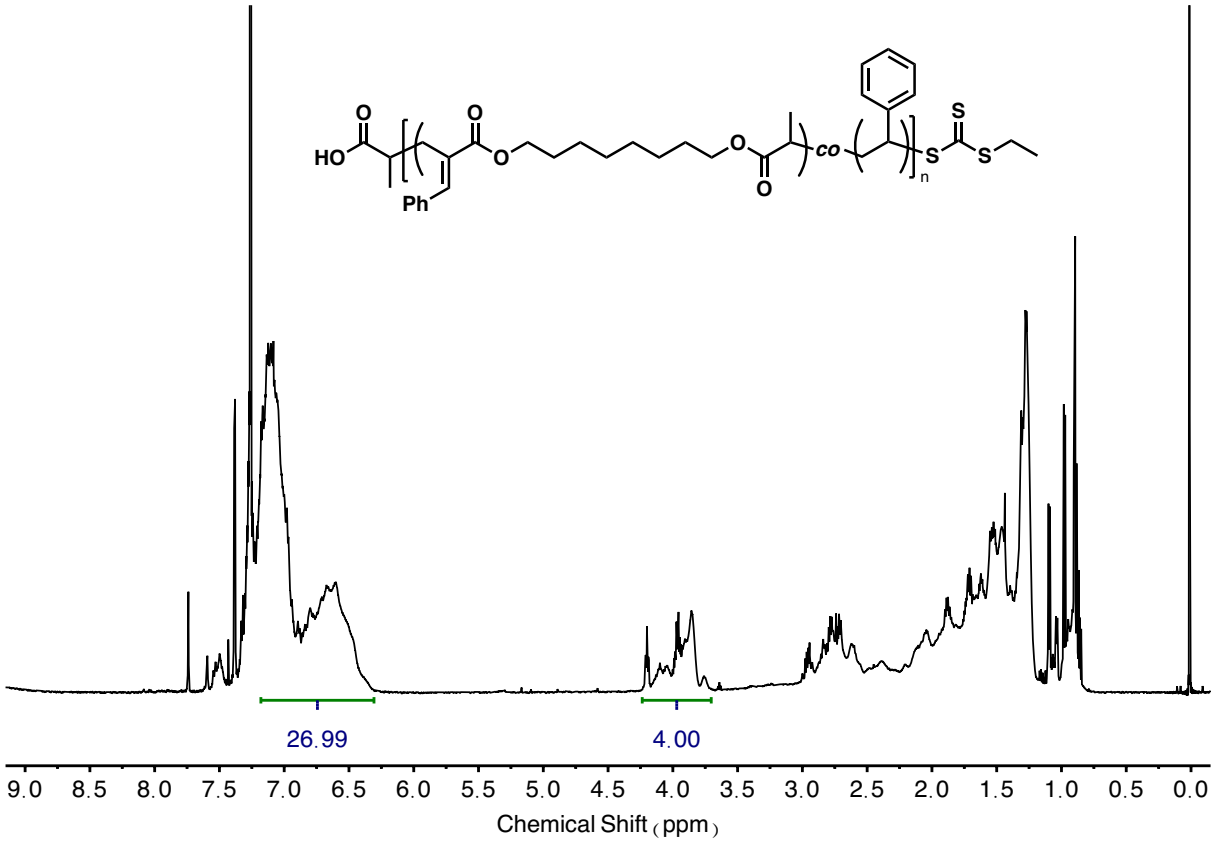

^{1}H NMR of degradable vinyl copolymer **P-1-*co*-MMA** at f_1^0 = 0.09.